Sediment mobility over a dispersive inner shelf from combined wave and tide bed shear stress

Déborah Belleney, Nicolas Le Dantec, Pascal Le Roy, Alain Hénaff

Sediment mobility over a dispersive inner shelf from combined wave and tide bed shear stress

Déborah Belleney[a*], Nicolas Le Dantec[b,c], Pascal Le Roy[b], , Alain Hénaff[a]

[a] Institut Universitaire Européen de la Mer, Geomer - UMR 6554 CNRS LETG, 29280 Plouzané, France

*deborah.belleney@univ-brest.fr

[b]Institut Universitaire Européen de la Mer, UMR 6538 Géosciences Océan, Technopôle Brest-Iroise, 29280, Plouzané, France

[c] Institut Universitaire Européen de la Mer, UMS 3113, Technopôle Brest-Iroise, 29280, Plouzané, France

Abstract

The sediment transfers that take place between the beach and the depth of closure on the inner continental shelf play a major role in the evolution of sandy shores at different time scales. The depth of closure of the foreshore sedimentary prism, which is generally dependent on wave conditions, remains poorly constrained in the context of an internal macrotidal platform. This work aims to define and evaluate this theoretical depth, which delimits the extension of sedimentary exchanges, in particular by including the constraints applied on the sea bottom by the tidal circulation, which are very strong on the inner continental shelf of western Brittany. The use of wave (WAVEWATCH III®), tidal (MARS3D), and bottom sediment (EMODnet) databases allows us to follow an original cartographic approach to study closure depths, based on the formulations of Hallermeier (1978 and 1981) and Soulsby (1997). This cartographic

approach is adapted to a spatial analysis of sediment mobility on a regional scale. First, the depth of closure shows a regional spatialisation of the seaward extension of the sediment mobility zone according to exposure to different wave climates and tidal ranges. Secondly, the method for calculating the depth of closure with the combined shear stresses (wave and tide), applied at the scale of the internal platform of western Brittany, allows the identification of three areas of movement of sedimentary particles according to critical mobility thresholds: 1) Area of no motion; 2) Area of transport and deposition; 3) Area of transport without deposition. The main contribution of this work is to propose at distinction between 2 offshore sediment motion limits, the transition to the upper plane bed (DoT_{upb}), and the incipient motion of particle (DoT_{motion}). In addition, this study confirms the potential of transport and deposition of sand particles at depths greater than 100 m in the most hydrodynamically intense areas, which implies the possibility of interconnections between hydro-sedimentary cells, through bypassing of headlands and crossing over rocky outcrops.

Keywords

Depth of closure, Depth of transport, Bed shear stress, Initiation of motion, Area of sediment transport and deposition, tidal and wave forcing

1. Introduction

The evolution and functioning of sedimentary coastal areas are strongly dependent on long-shore and cross-shore sediment transfers that operate within hydro-sedimentary cells (Komar, 1996; Pinot, 1998; Cowell et al., 2003; Héquette and Aernouts, 2010; Aagaard et al., 2011; Hénaff et al., 2015). These cells extend seaward over the inner continental shelf to the depth of closure. They are laterally delimited by geomorphological obstacles, such as headlands, river outlets, and submarine canyon heads, or by an inversion of the direction of the littoral drift determined by changes in the orientation of the coastline or the bathymetry.

The depth of closure is considered as a morpho-sedimentary boundary separating an active shoreface area from a more inactive offshore area, thus delineating the base of the nearshore prism. Determining its location is fundamental for assessing the long-term sediment budget of coastal systems (Allen, 1968; Swift, 1976; Barnard et al., 2013; Preston et al., 2018; Anthony and Aagaard, 2020; Hamon-Kerivel et al., 2020). Its application in coastal engineering is also used to delineate potential source areas of sedimentary material for beach nourishment operations, or for dredging waste. However, a number of recurring questions remain open. To what extent is the foreshore sedimentary prism actually closed? Can sediments of a littoral cell bypass headlands toward an adjacent cell, thus establishing a connection between cells? Several studies have confirmed this possibility, in particular along coastlines with intense hydrodynamic conditions, and underline the role of sediment transfers between littoral cells when assessing coastal sediment budgets (Valiente et al., 2019 ; Klein et al., 2020 ; Silva et al., 2021 ; King et al., 2021 and McCarroll et al., 2018 and 2021). Therefore, estimation of the depth of closure is critical to understand sediment dynamics in littoral cells and predict how coastal areas will respond to sea-level rise induced by climate change, as well as for the management of nearshore sediment resources.

The delineation of the shoreface, adjacent compartments, and associated depths of closure is still discussed due to the complexity of the determination methods (Anthony and Aagard, 2020). The definition of these boundaries is also subject to debate. For this study, the compartments considered between the external limit of the lower shoreface and the beach are (Figure 1) : i) the lower shoreface extending between the fair weather wave base and the base of the extreme wave significant changes in the beach profile; ii) the upper shoreface extending between the base of the extreme wave significant changes in the beach profile and the mean low tide level (Cowell et al., 1999). Hence, the upper shoreface records significant seasonal morphological changes, while the lower shoreface does not, even if intense seabed agitation

76 occurs under large wave conditions. For offshore compartments, this study considers the
77 offshore-transition zone as extending between the fair weather wave base of the lower
78 shoreface external limit and the extreme wave base offshore proximal limit (Reading, 1996,
79 and Nichols, 2009).
80 Worldwide, many authors have worked on the determination of this depth of closure,
81 especially on coasts exposed to waves and/or subject to strong tidal ranges (e.g. Hallermeier,
82 1978 and 1981; Birkemeier, 1985; Nicholls et al., 1997 and 1998b; Capobianco et al., 2002;
83 Robertson et al., 2008; Cerkowniak et al., 2015; Ortiz and Ashton, 2016; De Figueiredo et al.,
84 2019; Valiente et al., 2019 ; Hamon-Kerivel et al., 2020 ; Hamon-Kerivel et al., 2022). Two
85 main methods are used to locate it: field observations or calculation by empirical formulations
86 often applied using outputs of numerical models. Field observations are based on the repeated
87 acquisition of numerous cross-shore topo-bathymetric profiles of the beach and, above all, of
88 the bathymetry of the foreshore, yielding an envelope of significant morphological changes of
89 the littoral accumulations on annual to multi-year scales (e.g. Rozynski et al., 1998 ;
90 Roberston et al., 2008 ; Jabbar et al., 2015 ; Aragones et al., 2019). The observations can also
91 incorporate a geostatistical approach, combining median sediment size, D50, and textural
92 parameters (Aragones et al., 2018). On the basis of these field observations, empirical
93 formulations have also been developed. They take into account the wave conditions, the
94 nature of the bottom or the shear stresses exerted on the bottom by tidal currents and wave
95 orbital velocities (Hallermeier, 1978 and 1981; Birkemeier, 1985; Wright, 1995; Soulsby,
96 1997; Valiente et al., 2019; Coughlan et al., 2020; Hamon-Kerivel et al., 2022). Wave data,
97 which are the main input parameters of the formulations, can be obtained from in situ
98 measurements (e.g., nearbed current velocity profiles) or from wave model outputs (e.g.,
99 WAVEWATCH III®, or SWAN).

The depth of closure is expressed using different formulations, and is also associated with two different interpretations in terms of sediment mobility (Figure 1): i) DoC-envelope is computed using statistics of wave height and period from hindcast simulations and is interpreted as the limit of significant changes in beach profiles on a seasonal scale caused by storm wave action (Hallermeier, 1978); ii) DoC-motion is computed using statistics of wave height and period from hindcast simulations as well as grain-size parameters from seabed classification and is interpreted as the outer limit of sediment movements generated by fair weather waves (Hallermeier, 1981); iii) Depth of Transport (DoT) is based on wave and tide bed shear stress from hindcast simulations and was introduced by Valiente et al. (2019) who defined it as the limit of bed agitation corresponding to the upper plane bed transition under extremes hydrodynamic conditions. It is therefore of interest given the hydro-sedimentary conditions typical of the western Brittany platform.

This study examines the depth of closure at the regional scale of the western Brittany coastline, which is exposed to highly energetic hydrodynamic conditions. The study is based on the combined use of hydrodynamic (HOMERE for wave and MARS3D for tidal currents) and sedimentary (EMODnet) databases, allowing an innovative spatial mapping of DoC and an improved analysis of DoT that highlights the DoT_{motion}, defined as the limit of sediment motion transition. This study also aims to compare sediment mobility zones (no movement, transport and deposition and transport without deposition) during extreme and moderate wave conditions. Better understanding of sediment mobility in the inner shelf will improve our capabilities to estimate sediment fluxes, which is key to predictions of future changes in coastline position in response to climate change. Coastline position depends on the redistribution of sediments across the coastal zone to adjust to changes in sea level and wave climate.

2. Regional setting

The peninsula of western Brittany provides great diversity in the exposure of the coasts and the inner continental shelf, and this context is particularly interesting for the study of the limits of the coastal sedimentary prism at a regional scale. Northward, the peninsula is exposed to the conditions of the English Channel, westward to the Iroise Sea, and southward to conditions in the Bay of Biscay. The coastline exhibits diverse morphologies, consisting of coastal accumulations of limited extension (bays, inlets, pocket beaches) developed between rocky and soft cliffs, promontories, and various prominent headlands often associated with reefs and offshore islands (Figure 2).

Tidal ranges vary from 4.5 m to 8 m from the south to the north of the study area (Figure 2). Tidal surface currents can reach a maximum speed of 4.2 m/s in the Fromveur Channel. Mean speeds are less than 0.5 m/s over the entire inner shelf (< 30 m) and less than 0.25 m/s in the coves (DATA-SHOM- https://data.shom.fr). The coastline of western Brittany is exposed to three main wave climates (Figure 2, waves roses) : 1) on the northern coast, the prevailing wave direction is from the north-west, average significant height (Hs) is 1.5 m, reaching a maximum of 9.2 m; 2) on the western coast, the prevailing wave direction is from the west-south-west, with an Hs of 1.5 m and a maximum of 9.5 m; 3) on the southern coast, the prevailing wave direction is from the west-south-west, with an average Hs of 0.8 m with a maximum of 6.8 m.

The coastal prism is made of fine to coarse sands, with a significant biogenic fraction. Their accumulation results both from the remobilization of continental shelf deposits during the last transgression (Flandrian) and from the erosion of rocky coastal cliffs composed of granitic and metamorphic Hercynian rocks (Cagnard, 2008).

The EMODnet (2016) classification of the nature of the seabed (1/ 250 000 scale) into five classes (Figure 3) shows a variable distribution according to the three seaboards of western

Brittany: 1) the northern coast is mainly composed of outcropping bedrock, punctuated by patched of coarse to medium sands; 2) the west coast is more heterogeneous, with alternating patches of fine and coarse sand, as well as large rocky outcrops. Patches of muddy sediment are present in the south of the Molène archipelago (9), in the Bay of Douarnenez (15), and off Audierne Bay (17); 3) the southern coast also has a rocky basement dotted with patches of coarse to medium sediments, in particular in the alignment of the Bay of Bénodet (19) and the Glénan archipelago (20). Fine sediments dominate offshore and in Concarneau Bay (21), which connect to the north-western end of the large muddy belt (*Grande Vasière*) of the median platform of the Bay of Biscay.

3. Data and methods

This study focuses on the position (distance from the coast and depth) of the outer boundary of the coastal sedimentary prism of western Brittany. Its position is determined using three formulations: 1) DoC-envelope (DoC_{env}) calculated from Hallermeier (1978); 2) DoC-motion (DoC_{motion}) calculated from Hallermeier (1981); 3) DoT (motion and upper plan bed) measured from the combined wave and tidal bottom friction velocities (Soulsby, 1997) (Figure 4).

3.1. Depth of closure formulations: DoC-envelope and DoC-motion

To calculate limit depth for appreciable sand level changes by yearly extreme waves, Hallermeier (1978 and 1981) proposes a formulation (eq. 1) based on wave climate parameters. It is considered as the outer limit of the upper shoreface and represents the depth of the equilibrium envelope of profile change - DoC_{env} (Hallermeier, 1978).

$$DoC_{env} = 2.28\,He - 68\,(He^2/[gTe^2]) \quad (1)$$

Where *He* (m) is the significant wave height exceeded for 12 hours per year, *Te* (s) is the associated wave period (T02) and *g* (m/s^2) is acceleration of gravity (Figure 4).

Hallermeier (1981) suggests a second formulation to take into account a longer time scale (applicable for 10^2-10^3 years or longer) (Stive and de Vriend, 1995). It defines the lower shoreface limit or Depth of Closure motion (DoC_{motion}). It takes into account the grain size and is defined as follows:

$$DoC_{motion} = (Hs\text{-}0.3\sigma_s)\ Ts\ (g/[5000D_{50}])^{0.5} \quad (2)$$

Where *Hs* (m) is the annual mean significant wave height, σ_s is the associated standard deviation, *Ts* (s) is the mean significant wave period (T02) and *D50* (m) represents the median grain size (Figure 4).

Hallermeier (1978) recommends that tidal effects could be taken into account by using the mean low water level as a reference instead of the mean water level, thus allowing the consideration of the maximum extension of DoC (envelope and motion) towards the open sea. Therefore, all the wave parameters necessary for the DoC_{env} and DoC_{motion} calculations were extracted by considering only the periods of low water spring tides (LWS) over the period 1994 to 2016.

3.2. Depth of transport: DoT

The DoT is determined by comparing the combined bed shear stress and the threshold of motion, which is defined using the Shields mobility number. To account for the nonlinear interaction between wave and current boundary layers, Soulsby (1997) proposes the following expression to define the maximum bed shear stress, which can be used to determine the

threshold of sediment motion. Herein referred to as the "combined bed shear stress : τ_{comb} (N/m²)" (eq. 3) :

$$\tau_{comb} = [(\tau_m + \tau_w |\cos \emptyset|)^2 + (\tau_w \sin \emptyset)^2]^{1/2} \quad (3)$$

where τ_m (N/m²) is the mean bed shear stress (eq. 4), τ_m (N/m²) is the wave bed shear stress and φ is the angle between the directions of wave propagation and current.

The mean combined bed shear stress τ_m (N/m²) is derived from the current bed shear stress τ_t (N/m²) and the wave bed shear stress τ_w (N/m²) (eq. 4) and can be used to evaluate defined the sediment diffusion very near the bed:

$$\tau_m = \tau_t [1+1.2 (\tau_w / (\tau_t + \tau_w))^{3.2}] \quad (4)$$

Soulsby (1993) indicates that the response time of a sand grain in bedload motion is short compared to a tidal and wave period, and in this case we consider long wave periods under extreme conditions. This allows us to consider that the combined tidal and wave bed shear stress is representative of a stationary stress (steady current).

The tidal current bed shear stress τ_t (N/m²) (eq. 5) is derived from the near-bed friction velocity U_* (m/s) which is estimated using logarithmic profile method by considering a turbulent regime (eq. 6).

$$\tau_t = \rho U_*^2 \quad (5)$$

$$U_* = U(z)\, k / \ln (Z/Z0) \quad (6)$$

Where: ρ (1025 kg/m^3) is the density of water; k is the Karman constant (0.4); $Z0$ (m) is the bottom roughness parameter related directly to the median grain size D_{50} with the relation $Z0$

224 = D_{50} /12; Z (m) is the height above sea bed, and $U(z)$ (m/s) is current velocity at height Z
225 (Figure 4).
226
227 The wave shear stress is associated with the orbital velocity of the wave on the bottom and is
228 expressed as:
229 $\tau_w = 1/2\, f_w\, \rho\, Uw^2$ (7)
230 Where f_w is the wave friction parameter ($f_w = 1.39\ (A/Z0)^{-0.59}$) which depends on the semi-
231 orbital excursion under waves ($A = U_w\ T/\ 2\pi$) with ($T=T02$), and $U_w = \sqrt{(2U_{rms})}$ with U_{rms}
232 (m/s) as the root-mean-square wave orbital velocity at the sea bed.
233
234 The initial motion of a sediment occurs when the bed shear stress exceeds the critical stress τ_{cr}
235 corresponding to the threshold for initiation of movement. Following the approach developed
236 by Shields (1936), the Shields mobility number (θ) is the ratio of the shear stress (τ) acting on
237 a grain to move it and the immersed grain weight:
238 $\theta = \tau\ /\ (g\ (\rho_s - \rho)\ D_{50})$ (8)
239 Where: ρs (2650 kg/m^3) is the density of sediment
240
241 The threshold of initial motion is given as a critical value θ_{cr} of the Shields number, which
242 depends on the grain size (eq. 8). This critical value is determined from observations. For
243 large non-cohesive sediments (greater than a few mm), the value θ_{cr} = 0.06 proposed by
244 Shields (1936) has long been used as a reference. Since then, many authors have proposed
245 different values such as θ_{cr} = 0.047 (Meyer-Peter and Muller, 1948), θ_{cr} = 0.048 (Grant and
246 Madsen, 1982) or θ_{cr} = 0.055 (Soulsby, 1997).
247 It appears that implementation of one or other of the values has little qualitative influence on
248 the mobility areas defined below. Following previous studies (Valiente et al., 2019 and Grant

249 and Madsen, 1982), we use the critical threshold of 0.048 for the Shields mobility number in
250 this study.
251
252 From this critical threshold of motion, sediment transport rapidly leads to the emergence of
253 bedforms, the size of which depends on flow velocity. The length and morphological
254 characteristics of these sedimentary structures reflect the equilibrium with the sediment
255 transport capacity of the flow towards which they have evolved, and which depends on the
256 grain size and flow velocity (Moss, 1972; Southard and Boguchwal, 1990). Once the current
257 increases until it reaches the upper bed transition, the bedforms crests are trimmed and then
258 flattened and the seabed becomes more flat. The particles are scarcely deposited on the
259 bottom anymore and are mainly transported in suspension. The value of the Shields number
260 corresponding to this transition is θ=1. In this study, the DoT calculated with θ_{cr} = 0.048 is
261 designated as DoT_{motion} and the DoT calculated with θ_{cr} = 1 is designated as DoT_{upb}.
262 The depth of closure is meant to represent the furthest extent of sediment displacement.
263 Consistently, when exploiting the DoT calculations and the sequence of areas of movement
264 that are derived in this approach, we retain the limit of sediment motion (DoT_{motion}) as the
265 depth of transport. This definition differs from (Valiente et al., 2019) who define the DoT as
266 the upper plane bed transition DoT_{upb}. To further exploit the advantage of the spatial
267 representation of sediment mobility that is offered with the DoT approach, we analyze the
268 sediment transport in the inner shelf in terms of the areas of sediment movement defined as
269 :1) Area of no motion when θ < 0.048; 2) Area of Transport and Deposition (ATD) when
270 0.048<θ<1 ; 3) Area of Transport Without Deposition when θ> 1 (Figure 4).
271 The bed shear stress increases shoreward, often reaching a maximum before decreasing closer
272 to the beach. This is typically the case in more protected coastal environments (i.e.,
273 embayments, as opposed to rocky coasts that are more directly exposed to waves), where the

bed shear stress goes under the upper plane bed threshold, allowing the potential of a second, internal, DoT_{upb} limit and of a second, internal, ATD.

The two depths of transport (DoT_{motion} and DoT_{upb}) and three associated areas (no motion, ATD and ATWD) are calculated for different grain sizes (0.05, 0.5 and 2 mm), using equations (3) and (8) with the corresponding "critical" bed shear stress values for initial motion and upper plane bed (Table 1).

3.3. Hydrodynamic and sediment input data

The databases used to obtain wave parameters, tidal current, and granulometry, required for these calculations at the scale of western Brittany, are respectively the HOMERE database (developed by Ifremer, Boudière et al., 2013), the MARS3D database (Lazure and Dumas, 2008) and the EMODnet-Geology seabed substrate (European Marine Observation and Data Network initiated by the European Commission in, 2009) (Figures 4 and 5).

The HOMERE database (http://doi.org/10.12770/cf47e08d-1455-4254-955e-d66225c9dc90), newly accessible from the RESOURCECODE marine data toolbox, was built from the WAVEWATCH III® model. The de-structured triangular grid of the WAVEWATCH III® model allows the resolution of the grid to be adapted to different scales ranging from the coastal zone (refined meshes at ~200 m) to offshore (meshes of ~10 km) (Christophe et al., 2017) (Figures 4 and 5). The advantage of this model is that it provides data on a regional scale. However, the quality of wave prediction by the HOMERE model is insufficient in shallow waters (between 0 m and 10 m). Indeed, when approaching the coast, the local changes in wave propagation, such as reflection or diffraction phenomena behind artificial structures, are poorly simulated by offshore models like WW3 (Latteux, 2008). The results presented below are therefore not representative of the surf zone. The purpose of this study is

299 to improve the determination of the offshore limit of sediment remobilization. For the DoC_{env}
300 and DoC_{motion} methods, wave heights (Hs and He) and associated periods (Ts and Te) were
301 extracted over the period from 1994 to 2016 at the isobath -30 m. For DoT method, bottom
302 friction velocities (Urms, rms of bottom velocity) were extracted under two wave conditions:
303 extreme (or « storm ») and moderated. Extreme conditions are represented by the significant
304 wave height exceeded for 12 hours (He) during February 2014, since it is the month during
305 which the coastline was the most impacted in the last decade (Blaise et al., 2015 ; Stéphan et
306 al., 2019). Indeed, during this period, most of the Atlantic coast of Europe experienced the
307 most extreme weather conditions for the last 50 years (Masselink et al., 2016 ; Castelle et al.,
308 2018). Moderated wave conditions correspond to the 10^{th} quantile (Hq10) over the month of
309 February 2014.
310 The MARS3D (Model for Applications at Regional Scales) database was used to compute the
311 near-bed friction velocity U_* associated with the tide-induced current, used for the calculation
312 of the DoT. The resolution of the square grid of the MARS3D model is 500 m for western
313 Brittany (Figure 5). The near-bed friction velocity U_* is derived from the velocity in the
314 bottom layer and the roughness scale provided in the model output, using equation (6). Tidal
315 current bed shear stress was computed over only one tidal cycle, during the largest spring tide,
316 on 1 February 2014, again, retaining the maximum value at each node. On this same date, the
317 water level in Brest reached 7.40 m, a value higher than the water level during mean high
318 water spring, which is 7.05 m (DATA-SHOM - https://data.shom.fr).
319 Tide and wave bed shear stress are calculated from equations 5 and 7, during extreme
320 conditions (February 2014 and Largest spring tide), which represents an extreme scenario
321 with a 10-year return period. This scenario is close to a storm that would occur at the same
322 time as spring tides, which is very rare, and is representative of maximum sediment mobility
323 over decadal time scales. The two models of MARS3D and WAVEWATCH III® do not have

the same grid size. In order to solve this problem for the DoT calculations, the points of the WAVEWATCH III® node, which are denser near the coast, are used as a reference (this represents 13 051 points). From the values calculated using the MARS3D outputs, the shear values due to the tidal current U are assigned to each node of the WAVEWATCH III® model using the nearest neighbour method. The final grid including wave, tidal, and grain size data is therefore that of the WAVEWATCH III® model. Final DoT maps are generated using kriging interpolation (12-point search near each point and 500 m distance).

The particle size classes were obtained from EMODnet seabed substrate by extracting values from this raster (e.g. sand) at each node of the HOMERE database (WAVEWATCH III® model), and converting them to D50 (for "No data at this level of Folk" and "mixed sediment" a D50 of 0.5 mm was used) (Table 2).

4. Results

4.1. Wave height and grain size as factors of depth of closure variabilities along the western Brittany coastline

The DoC_{env} and DoC_{motion} were calculated for 68 points along the western Brittany coast, using 23 years of WAVEWATCH III® wave model (height and period) and EMODnet grain size data, at the -30 m contour. The period Te vary between 6.6 s and 15.4 s while Ts vary between 3.7 s and 7.9 s (Figure 6-A and Table 3). The mean wave periods are 10.8 s for Te, with a standard deviation of 0.9 s, and 5.8 s for Ts with a standard deviation of 0.7 s. The values of Te are approximately twice as large as the values of Ts. Extreme wave heights (He) vary between 1 m and 6.8 m, while mean significant wave heights (Hs) vary between 0.5 m and 2.5 m along western Brittany (Figure 6_B and Table 3). The minimum difference between He and Hs values is around 2 m and is observed in the less exposed areas (Figure 6_C): Concarneau (21), Douarnenez (15), east of Ouessant (7), and Lannion Bay (1). The

maximum difference between the values of He and Hs is of the order of 4.5 m and is observed in most exposed areas: Glénan (20), north of Audierne Bay (17), Portsall (6), and Batz Island (3).

The results obtained for the DoC_{env} along the west coast vary between 4 m and 12 m with minimum values of 4 m to 5 m in the bays of Concarneau (21) for the south coast, Douarnenez (15), and in the shelter of Ouessant Island (7) for the west coast (Figure 6_D and Table 3). On the contrary, high values of DoC_{env}, greater than 10 m depth, are registered around the Glénan archipelago (20), north of Audierne Bay (17), south of the Molène archipelago (9), towards Portsall (6), and around Batz Island (3). Along the northern coast (excluding Batz Island), the DoC_{env} gradually decreases from west to east, from 12 m to 6 m.

The DoC_{motion} is much higher, and has a much greater variability than the DoC_{env}, ranging from 9.5 m to 65 m (Figure 6_D and Table 3). The western coastline shows particularly strong fluctuations in DoC_{motion}, with values ranging from 9.5 m to 65 m (i.e. the whole range of western Brittany). However, the relative evolution of the DoC_{motion} along the coasts of western Brittany is similar to that of the DoC_{env}, with minimum values in the bays of Concarneau (21), Douarnenez (15), and in the shelter of Ouessant Island (7), and high values around the Glénan archipelago (20), north of Audierne Bay (17), south of the Molène archipelago (9), towards Portsall (6) and around Batz Island (3). Along the northern coast (excluding Batz Island), the DoC_{motion} also shows a progressive decrease from west to east, from 30 m to 25 m. DoC_{motion} variability is partly related to the changes in sediment grain size, to which it is sensitive, and which induces discontinuities, unavoidable with the methodology followed for this study. The high DoC_{motion} values in Concarneau Bay and at the southern limit of Douarnenez Bay seem to be related to a small grain size (0.05 mm).

374

375 **4.2. Contributions of waves and tide to combined bed shear stress**

376 Extreme wave heights (He) exceeded for 12 hours during February 2014 (Figure 6-A) were
377 high offshore (between 9 m and 12 m) and gradually decreased to generally no less than 4 m
378 near to the coast (< -20 m depth) and in well-sheltered bays (9, 15 and 21). Moderated wave
379 height (Hq10) varies from 4 m to 7 m offshore and gradually decreases to generally less than
380 1.5 m at the coast (< -20 m/-30 m depth) (Figure **7**-B). More specifically, Hq10 are 1.5 time
381 lower than He in the south and west and twice as low in the north (Figure 6 and 7). Compared
382 to the mean significant wave (Hs), the Hq10 values are 0.5, 0.6, and 0.8 sizes higher in the
383 south, west, and north, respectively (Figure 6 and 7). Tidal-induced bottom current velocities
384 (U-tide) reach 3.43 m/s in the straits, such as around the islands of Ouessant (7) and Batz (3),
385 and in the Four (10), Fromveur (8) and Raz de Sein (16) channels (Figure 7-C). In general, the
386 offshore friction velocities increase from south to north, from 0.16 m/s to 1.5 m/s, in line with
387 the increase in tidal range. Approaching the coast (around 0 to -20 m), friction velocities
388 remain below 0.5 m/s over the entire part of western Brittany and below 0.15 m/s in the Bays
389 of Concarneau (21) and Douarnenez (15).

390

391 The mean extreme wave bed shear stress (τ_{waveHe}) is 11.1 N/m² with higher values > 30 N/m²
392 around capes, islands, and near the coastline, particularly close to the rocky outcrops that
393 extend offshore (beyond -50 m) (Figure 8-A). Otherwise, τ_{waveHe} logically decrease in the
394 most sheltered areas, with minimum values < 3 N/m² in the Bay of Brest (13) as well as in the
395 Douarnenez (15) and Concarneau (21) bays.
396 The tidal bed shear stress (τ_{tide}) is lower by a factor of 35 than extreme wave bed shear stress
397 with a mean value of 0.4 N/m² (Figure 8-B). The maximum τ_{tide} reach 13 N/m² in straits (16,
398 10 and13) and around islands (3, 7 and 8). They correlatively increase relative to the tidal

currents with values lower than 0.5 N/m² in the south, from 0.5 N/m² to 1 N/m² in the west, and up to 7 N/m² in the north.

The combined bed shear stress during extreme waves (τ_{combHe}), is high over the entire shelf, with a median value of 7.6 N/m² (Figure 8-C). The difference with τ_{waveHe} is more pronounced in the north, with values higher by + 0.5 N/m² to + 5 N/m², while in the west and south, values are higher by + 0 N/m² to + 0.5 N/m². Specifically, combined bed shear stress (τ_{combHe}) tends to be significantly higher than the stresses induced by the waves alone (τ_{waveHe}) in the tidal channels or straits (+5 N/m² to +10 N/m²). Extreme level combined bed shear stresses, greater than 30 N/m², presents a qualitative correlation with sediment distribution (Figure 8-C).

In comparison, the combined bed shear stress obtained from Hq10 ($\tau_{waveHq10}$) are lower than τ_{combHe} with maximum value of 39 N/m² (Figure 8-D) and mean value of 3.45 N/m². Therefore, $\tau_{waveHq10}$ is 10 times greater than τ_{tide} nevertheless 2.8 times smaller than τ_{combHe}.

4.3. Threshold of motion (DoT)

In the first part of this section, the results for the areas of sediment mobility (no motion, transport and deposition and transport without deposition) are shown for bed shear stress induced by wave during extreme and moderated conditions (He and Hq10) and by tide separately, and for sandy particles (0.5 mm). In the second part, the results for the areas of sediment mobility are shown for combined bed shear stress during extreme and moderated wave conditions, for three grain sizes (0.05, 0.5 and 2 mm). Separating each type of sediment to obtain a representation over the whole area (not constrained by the type of sediment) makes it possible to observe the fate of sediments without presupposing the location of sources, also to identify the areas of transport without deposition.

Under the influence of only the extreme waves (He), the ATD_{WHe} (Figure 9-A) shows that sandy particles (0.5 mm) can be transported and deposited over the entire study area, except

424 on rocky outcrops where the particles are only transported without being deposited. The sand
425 particles are not set in motion only in the Bay of Brest (13). Furthermore, under the
426 moderated wave conditions (Hq10) (Figure 9-B), the sandy particles (0.5 mm) are not be
427 transported over the entire study area, particulary in bays (13 and 15), in part of the southern
428 area as well as offshore, to the west (beyond the -30 m), and to the north. In addition, the area
429 of transport without deposition on the rocky outcrops is reduced in favour of the ATD_{WHq10}.
430 Under the influence of only tide, ATD_T (Figure 9-C) shows that, sandy particles (0.5 mm) can
431 be only transported and deposited on the western (beyond -50 m) and northern (beyond -
432 20 m) part of the area, and in the tidal channels or straits (10, 13 and 16).
433 Under extreme combined bed shear stress, all fine particles (0.05 mm) of EMODnet map can
434 be transported (Figure 10_A). However, these fine particles cannot be deposited under current
435 (modelled) conditions in some of the patches where they occur (Figure 10-A - green colour),
436 particularly those off Molène Archipelago (10). In this case, combined tide and wave friction
437 velocities are too high to allow the deposition of fine sediments. The same is applicable to
438 medium sediments (0.5 mm) of EMODnet seabed substrate map, which can be transported
439 and deposited almost anywhere, except in a few areas where deposition is not possible (Figure
440 10-B). Coarse particles (2 mm) can be transported and deposited over most of the studied area
441 except in the Bay of Brest (13) (Figure 10-C).
442 If the entire study area is considered, without taking into account the presence or absence of
443 sediments, fine and medium particles can be transported over the platform, while coarse
444 sediments cannot be transported in sheltered areas and to the south (Figure 10-D-E-F). In
445 addition, the areas of transport without deposition mainly correspond to the rocky outcrops of
446 the inner shelf platform for medium and coarse sands.
447

448 Under moderate conditions (Hq10), the areas of possible deposition of fine particles
449 (0.05 mm) are more extensive than during extreme wave conditions (Figure 11_A), for
450 instance off Molène Archipelago (10). For medium sand particles (0.5 mm), the areas of
451 transport and deposition are more extensive under moderate condition (Figure 11_E) and an
452 area where sediment mobility is no longer sustainable appears in the bay of Brest (13). With
453 the decrease in bed shear stress, coarse particles that were transported and deposited in
454 agitated periods cannot be in motion.
455 As in extreme wave condition, if the entire study area is considered, without taking into
456 account the presence or absence of sediments, the particles can be transport over the platform
457 and around the headlands, the islands and across rocky outcrops (Figure 11_D,E,F). This
458 indicates that exchanges between sediment patches, including bypass around headlands, are
459 possible if the patches are not too distant.
460

461 **4.4. Comparison between DoT and DoCs for headland bypassing**

462 In addition, to further enhance the assessment of potential sediment mobility at the scale of
463 littoral drift, it is necessary to move from a regional to a local scale. By focusing on an
464 embayment or cape (Figure 12), it is notably easier to compare the different depth of closures
465 (DoTs and DoCs). This approach was carried out for four representatives of the rocky
466 promontories and headlands encountered in western Brittany. The DoC_{env} is positioned
467 between -6 m and -13 m depth, at the level of the first or second slope break, and could be
468 equivalent to the internal DoT_{upb} for certain coastal configurations, such as Goulven (4),
469 Guisseny (5), and Sein (16). To the north, in the cases of Goulven (4) and Guisseny (5), the
470 DoC_{motion}, located in the middle of the rocky outcrops at a depth of 25 m (Goulven) and 34 m
471 (Guisseny), is shallower than the DoT, which extends to depths greater than 60 m, beyond this
472 rocky outcrop. To the west, at the Penmarc'h cape (18) and at the Raz de Sein (16), the

DoC_{motion} is located at 53 m and 27 m, respectively, while the transport and deposition area extends well beyond the rocky outcrops, beyond 70 m (Penmarc'h) and 45 m deep (Raz de Sein). Thus the determination of the ATD for these two areas, calculated following the DoT approach, reveals that sediment transport, which is supposed to be blocked by rocky headlands according to the DoC_{motion} approach, would in fact be possible during extreme conditions. Thus, the DoC_{motion} shows a limitation of bypass effects and transport and deposition possibilities on the rocky outcrops and beyond. As previously stated, in extreme conditions the DoT method indicates that there is no deposition of sediment in the upper shoreface for some beaches, as in the north of the Raz de Sein and near Penmarc'h Cape. This raises questions about the capacity of the beaches to accumulate sediment

5. Discussion

5.1. DoC-envelope (significant changes) and DoC-motion (fair weather wave base)

The results show a spatial distribution of the $DoC_{env,}$ which closely follows the configuration of the coastline (north, west and south): lower values correspond to the inner bays and higher values to headlands. In accordance with its calculation method (eq. 1), the variations in the DoC_{env} are directly linked to the sheltered or exposed nature of the point where the wave parameters (He) are measured. The DoC_{motion} also follow the wave height characteristics. Thus, the greater the wave height, the deeper the DoC_{motion}, except for certain isolated points, particularly on the western side. Overall, the DoC_{motion} is 3.6 times higher than the DoC_{env}. Specifically, the difference is greater (5 to 6 times) around headlands and islands exposed to waves. It clearly shows the potential remobilisation of sediments and the capacity of bypassing the headlands in the example of western Brittany, representative of a dispersive platform with reefs.

The DoC_{motion} values show a significant standard deviation of 11.8 m, revealing heterogeneity along the western coastline. These fluctuations in DoC_{motion} are linked to both spatial

variability of the wave conditions and the grain size without the apparent possibility of discriminating them, probably because they are two interdependent variables. Indeed, grainsize is driven, in part by wave and hydrodynamic conditions. Nevertheless, the control of grain size appears clearly in certain bays (Concarneau and Douarnenez) where, considering a constant low value of wave height, the depth of closure is doubled or even tripled according to the transition of a sandy grain size (0.5 mm) to a muddy grain size (0.05 mm). The same sensitivity can be observed on the north coast, around the island of Batz, where the change from coarse sand (2 mm) to medium sand (0.5 mm) twice the DoC_{motion}, for instance from 24 to 46 meter depth for nodes 51194 and 51274 as well as from 29 to 58 meter depth for nodes 53075 and 52258. The calculation of the outer limit of the shoreface is therefore very sensitive to grain size, which indeed strongly influences sand mobility. In order to better observe the sensitivity of the DoC_{motion} to grain size, it might be interesting to repeat the calculation with other grain sizes for the entire study area. For muddy sediments, a better consideration of the effect of cohesion on sediment mobility will mitigate the increased effect of the DoC. Although changes in sedimentary cover (grain sizes) can sometimes be very marked in results, more gradual changes should be expected in reality. The methodology followed, which is linked to the sedimentological data available, where the grain size is accounted for with discretization by classes, does not allow this gradual nature to be taken into account. Having input data that more accurately represents gradual changes in sediment cover would help to mitigate spatial discontinuities in the assessment of DoC.

In order to take in account the macrotidal context, the DoC calculations were computed for the MLLW (Mean Lower Low Water). However, whatever the tidal regime, the DoC data obtained in this study are consistent with those obtained on continental shelves exposed to extreme waves (Table 4). In fact, the higher the He, the higher the DoC_{env}. However, this is

not observed in Hamon-Kerivel et al., 2022 (Dingle Bay and Portstewart), which show an equivalent or even higher DoC_{env} for smaller He. This may be explained by the fact that the associated He for the Dingle Bay and Portstewart sites are higher than in our study. In addition, the previous study of Menier et al. (2019) on the relatively sheltered coast of south Brittany (mean significant wave < 2.5 m), shows a minimum DoC_{env} of 7 m and a maximum DoC_{motion} of 20 m. The values of DoC_{env} data are quite consistent at a yearly scale between west and south Brittany. In contrast, the mean DoC_{motion} values representative of sediment mobility on a decadal, or even centennial, scale are about 10 m deeper in west Brittany for medium sands (0.5 mm). The results suggest that extreme waves induce relatively homogeneous DoC_{env} at seasonal and annual time scales when considering the regions of west and south Brittany. In contrast, DoC_{motion} vary more significantly at a decadal time scale in response to the exposure to dominant wave and grain size variability.

5.2. Consideration of conditions of sediment transport and deposition across a macrotidal platform by the DoT calculation

The results on DoT_{motion}, confirme that sediment transfer can bypass rocky promontories/rocky reefs during extreme and moderate wave conditions as has already been highlighted in many recent publications (Valiente et al., 2019; Klein et al., 2020; Silva et al., 2021; King et al., 2021; McCarroll et al., 2018 and 2021). More locally, this study also confirms prior work of Chauris (1987) and Jabbar (2016), which suggests respectively that deep transits could occur in north and between the western and southern parts of western Brittany. In accordance with Valiente et al. (2019), the deposition and transport area obtained with the DoT approach at a regional scale shows that during extreme hydrodynamic conditions, sediments composed of medium to coarse sands are susceptible to be transported and deposited over a great distance from the coastline, up to 25 km to 40 km offshore

548 (maximum of the targeted study area), i.e. at depths > 100 m, much further offshore than the
549 DoC_{motion}. This pushes the theoretical extension of the lower shoreface far offshore, as
550 confirmed by the study conducted in SW England, where the depths of sediment motion are
551 exceeded across the entire domain. These results are also consistent with Mengual et al.
552 (2019), who showed that sandy sedimentary fluxes are possible all across the southern part of
553 the inner continental shelf of western Brittany up to depths greater than 130 m, particularly in
554 autumn and winter. These results raise questions about the relevance of DoT_{motion}, located far
555 offshore, as an external marker of the extension of the coastal domain in the present case of a
556 highly dispersive macrotidal platform. It appears that DoT_{motion} rather corresponds to the
557 lower limit of the upper offshore domain (offshore transition), limited at the top by the action
558 of fair weather waves and at the base by the action of extreme waves (Reading, 1996). It is
559 therefore more appropriate to consider DoC_{env} alone as representative of the extension of the
560 coastal domain (i.e the shoreface).
561 This study that compared DoT method under extreme and moderated waves conditions allows
562 examining tidal contribution. In fact, the change in sediment mobility from wave alone to
563 combined bed shear stress is very different under extreme or moderated conditions (Figure 10
564 and 11). That means, under moderate wave conditions, the changes in sediment mobility are
565 greater when comparing combined bed shear stresses with those due to waves only,
566 specifically in areas of largest tidal stress, i.e. offshore and in tidal channels. Thus, when
567 assessing the depth of closure with the DoT method, considering extreme wave conditions
568 will tend to mask the effect of tidal stresses. Moreover, due to the monthly recurrence of
569 spring tides, it is relevant to consider the effect of tidal stresses on sediment remobilization.
570 This is why, in the context of a macrotidal platform, it is preferable to calculate the DoT in
571 moderated wave periods (wave height equal to 3 times He or 1.6 times Hs).
572

5.3. Review of compartmentalisation of the inner continental shelf

The different formulations of depths of closure (DoCs and DoTs) allow us to investigate the behaviour of the distribution of sediment across the western Brittany shelf (Figure 13). In cases I and IV, the DoT_{motion} and the DoT_{upb} limits, are both located at the same place, i.e. halfway along the rocky basement outcrop. This configuration is valid for medium sands in moderated periods (Hq10 period) and for coarse sands during extreme periods (He). In case II, the DoT_{upb} is deeper than the DoC_{motion} and matches with the offshore limits of rocky outcrops to the north and south. This configuration is valid for medium sands in extreme periods. In case III, the DoT_{motion} matches approximately with the offshore rock basement boundary at about -50 m. This configuration corresponds to coarse sands in moderated periods, and the decrease in bed shear stress makes the DoT_{upb} disappear. However, in less turbulent periods, the remobilized coarse sands can be redeposited on the platform. Thus, previous results suggest that changes of roughness and bathymetry corresponding to the transition between rocky and sediments outcrops will therefore have an impact on the location of the different boundaries of sediment behaviour areas in addition to the combined effects of hydrodynamic conditions and the grain size. This result confirms the implication of seabed morphology on sediment mobility in the shoreface compartment, as shown by recent work by Hamon-Kerivel (2022).

This study has allowed to refine the depth of transport limits previously established (Valiente et al., 2019 and Hamon-Kerivel et al., 2020) according to the compartmentalisation of the inner continental shelf previously established by Reading (1996) and Cowell et al. (1999) (Figure 14). In fact, the important contribution of this work compared with previous studies, is the distinction between DoT_{upb}, which corresponds to the transition to the upper plane bed, and DoT motion, which corresponds to the start of particle entrainment.

598 -The DoC_{env}, i.e. the outer limit of significant movement considered as the envelope of the
599 beach profile, and calculated from the formulation of Hallermeier (1978), is positioned
600 between the upper and lower shoreface. It corresponds to the proximal extreme wave base
601 (Hallermeier, 1978) and shows variations on seasonal to annual scales.
602 -The internal DoT_{upb} can be equivalent to the DoC_{env} and corresponds to the end of the
603 envelope, where sediment deposition is no longer possible under energetic conditions.
604 -The DoC_{motion} boundary of the sedimentary movements, determined from the fair weather
605 waves (Hallermeier, 1981) corresponds to the boundary between the lower shoreface and the
606 transition-offshore zone, and shows decadal-scale changes.
607 -The DoT_{upb} can be equivalent to the DoC_{motion}, depending on the wave climate and the size of
608 the grains considered, as already noted by Valiente et al. (2019).
609 -The DoT_{motion} boundary, determined from the maximum shear stresses under extreme
610 conditions, corresponds to the boundary between the transition-offshore zone and the
611 offshore. It corresponds to the distal extreme wave base and displays changes related to
612 centennial storm events.

613 **6. Conclusion**

614 This study presents a comparison of the depth of closure calculated from wave parameters
615 (height and period) and wave and tide bed shear stress for both extreme and moderated wave
616 conditions on the western Brittany macrotidal continental shelf.
617 This study confirms that the DoT approach shows that sediment transfer can occur between
618 two littoral cells separated by a rocky outcrop or headland, deeper than 50 m. Compared to
619 the depth of closure (DoC_{motion}) approach, which seems to have more limited applicability
620 particularly on platforms with low sediment cover and rocky outcrops, the DoT method using
621 spatialization of the combined bed shear stress offers the advantage of taking into
622 consideration possible bypass effects between littoral cells in extreme conditions.

623 However, the DoT_{motion} limit, when calculated under extreme hydrodynamic conditions,
624 extends very far offshore. This limit does not appear to be optimal for establishing the outer
625 extent of the sedimentary prism, and rather corresponds to the transition-offshore limit and the
626 distal extreme wave base. The analysis under different wave conditions shows that the
627 DoT_{motion} is closer to the coast and that the sediment can be deposited more widely on the
628 upper shoreface during moderated conditions while in extreme conditions the areas of
629 transport without deposit are more extensive. Furthermore, it appears that applying the DoT
630 method with moderated wave conditions allows for a better understanding of the effects of
631 tidal currents on the remobilisation of sediment over a short time scale.

Figure 1

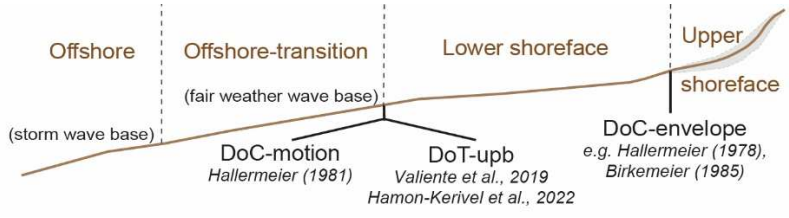
Offshore
Offshore-transition
Lower shoreface
Upper
shoreface
(fair weather wave base)
(storm wave base)
DoC-motion
Hallermeier (1981)
DoT-upb
Valiente et al., 2019
Hamon-Kerivel et al., 2022
DoC-envelope
e.g. Hallermeier (1978),
Birkemeier (1985)

636 **Figure 2**

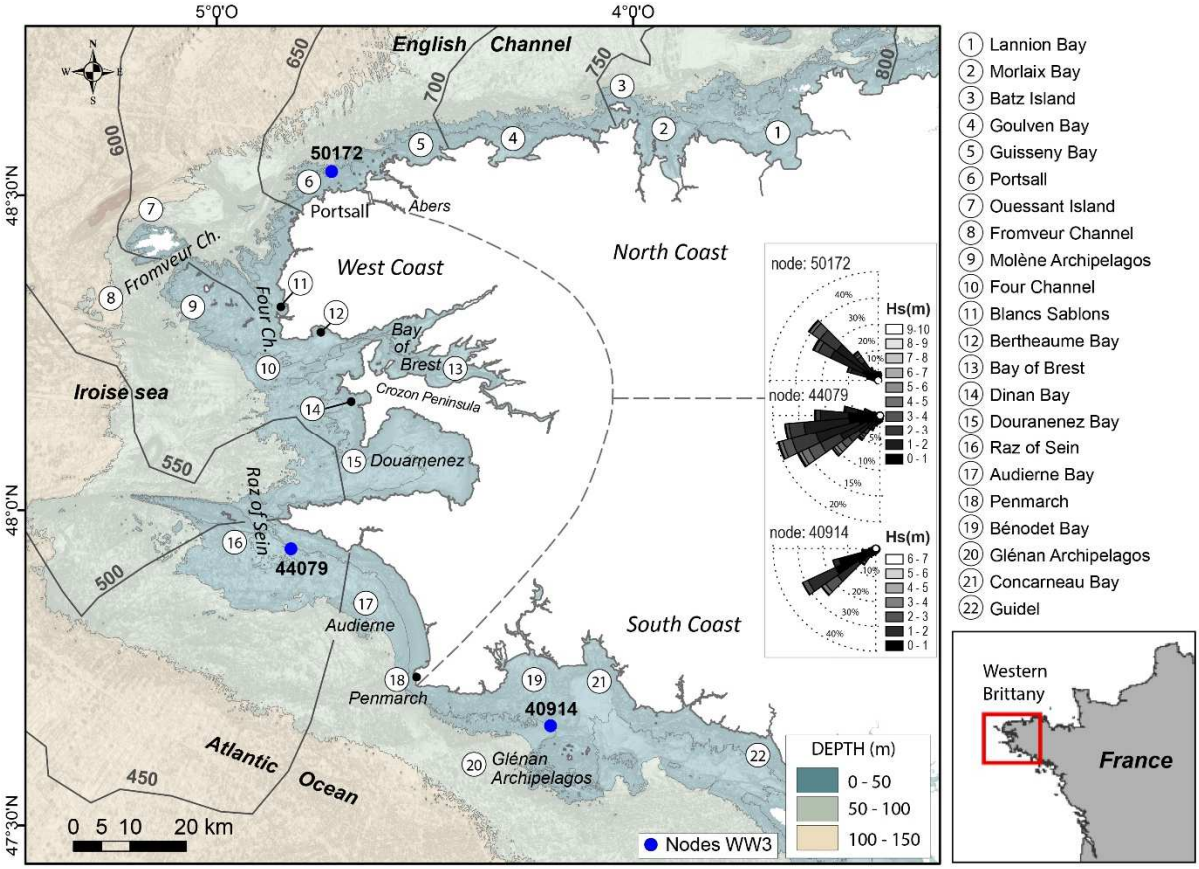

637

638

639

640 **Figure 3**

641

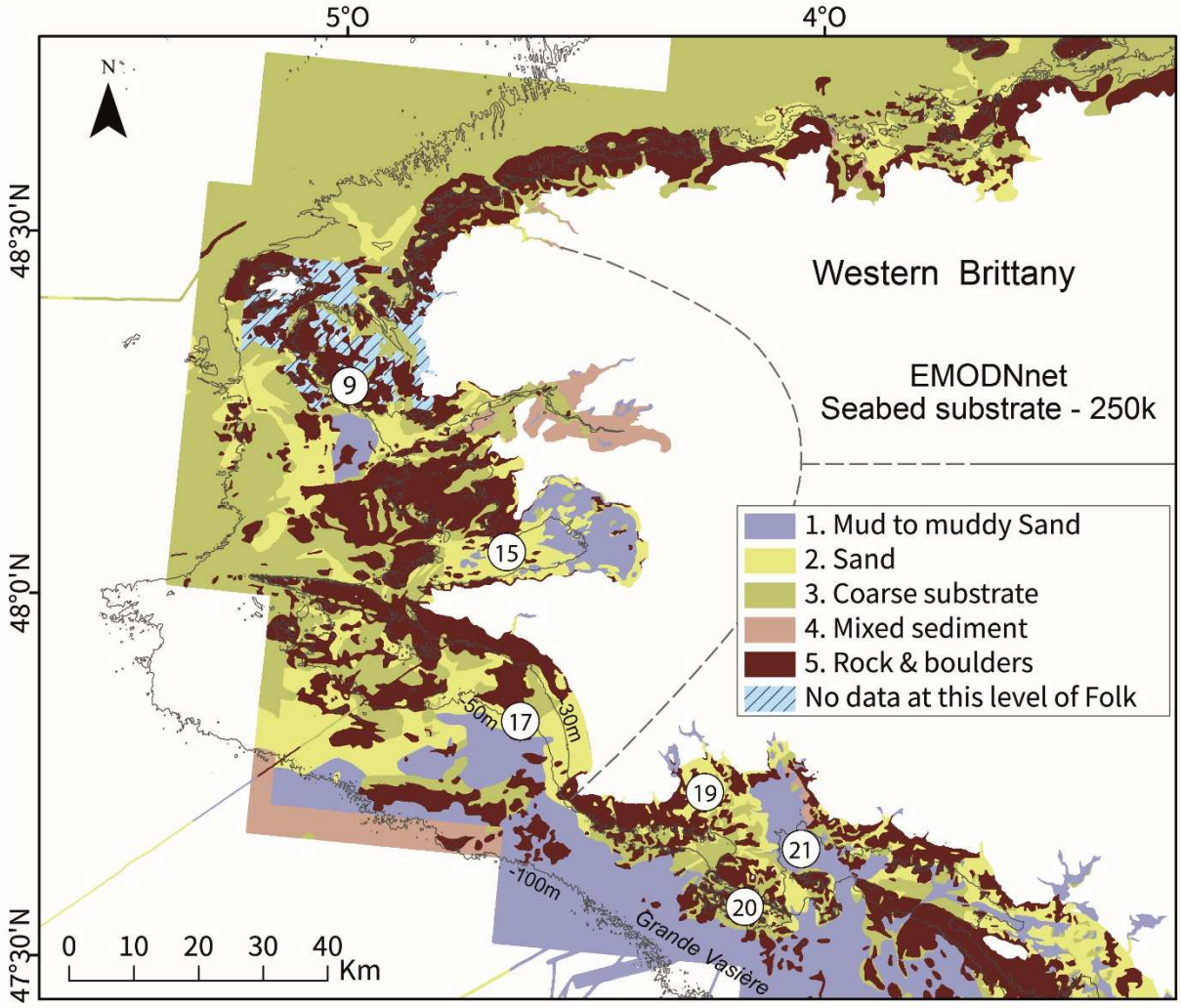

642

643

644

645

646 **Table 1**

647

Grain size (mm)	**0.05**	**0.5**	**2**
τ_{cr} for θ_{cr} = 0.048 (DoT motion)	0.038	0.38	1.5
τ for θ = 1 (DoT upper plane bed)	0.79	7.9	31.8

648

649

Figure 4

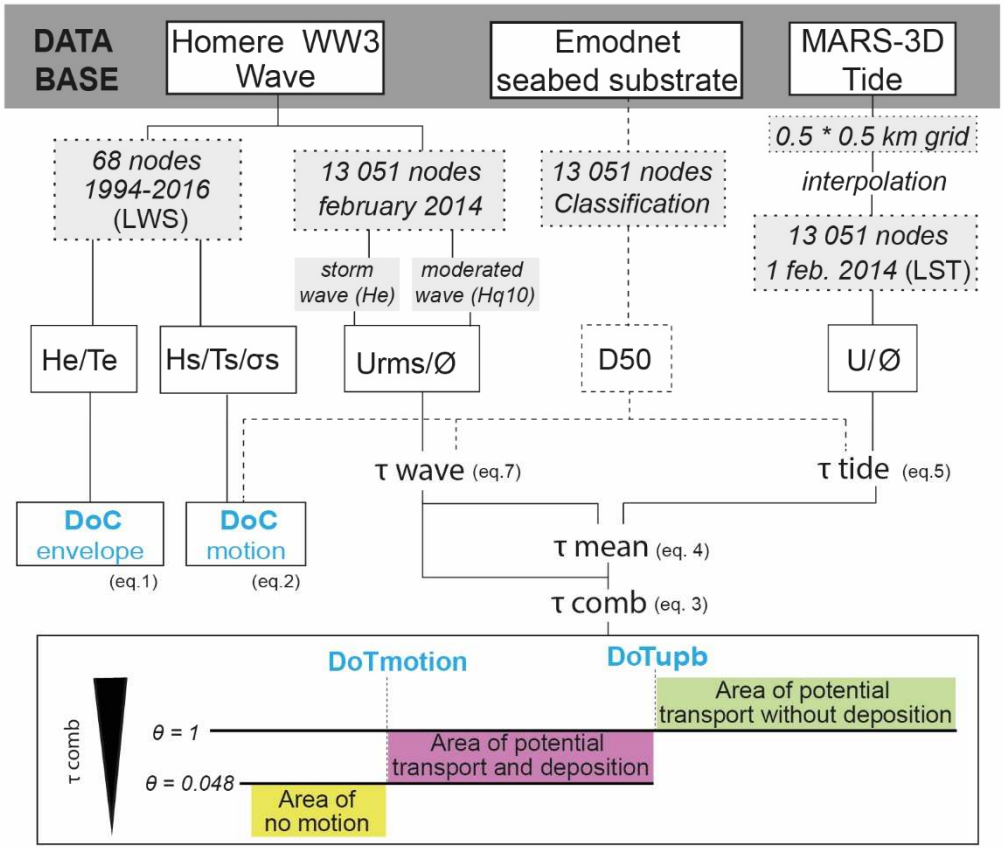
DATA BASE
Homere WW3 Wave
Emodnet seabed substrate
MARS-3D Tide
68 nodes 1994-2016 (LWS)
13 051 nodes february 2014
13 051 nodes Classification
0.5 * 0.5 km grid
interpolation
13 051 nodes 1 feb. 2014 (LST)
storm wave (He)
moderated wave (Hq10)
He/Te
Hs/Ts/σs
Urms/Ø
D50
U/Ø
τ wave (eq.7)
τ tide (eq.5)
DoC envelope
(eq.1)
DoC motion
(eq.2)
τ mean (eq. 4)
τ comb (eq. 3)
DoTmotion
DoTupb
Area of potential transport without deposition
τ comb
θ = 1
θ = 0.048
Area of potential transport and deposition
Area of no motion

655 **Figure 5**

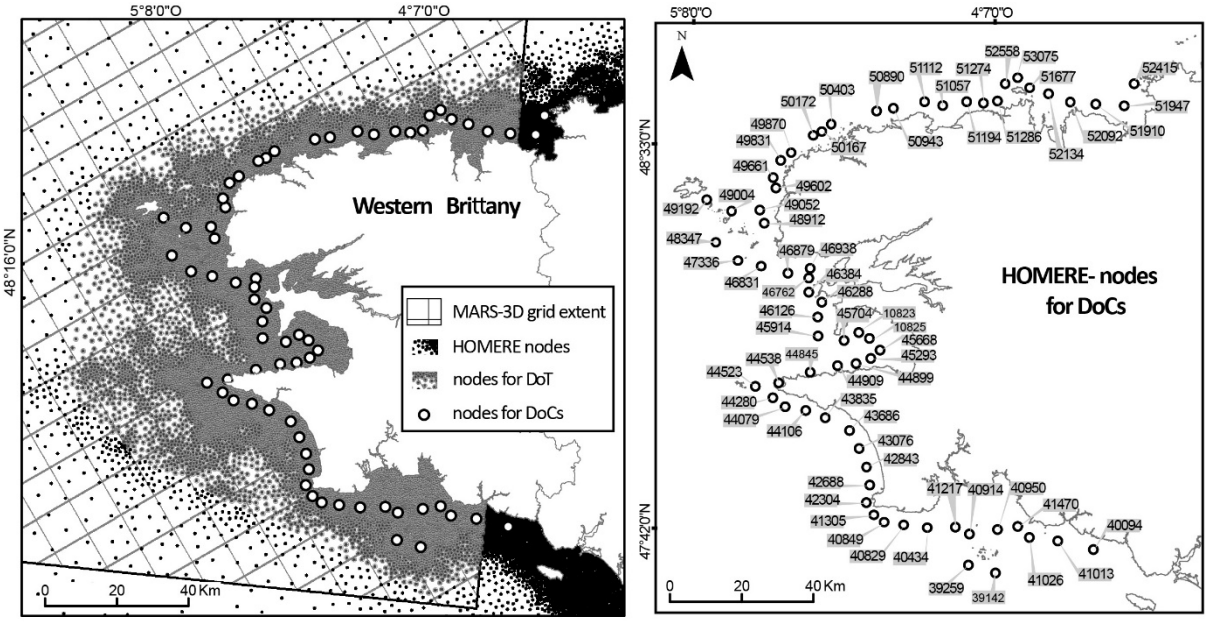

656

657

658

659 **Table 2**

D50 (mm)	Seabed substrate Edmonet
0.05	Mud to muddy Sand
0.5	Sand
2	Coarse substrate
20	Rock-boulders

660

661

662 **Table 3**

	DoCenv (m)	He (m)	Te (s)	**DoCmotion (m)**	Hs (m)	Ts (s)	D50 (mm)
Max	12	6.8	15.4	65	2.5	7.9	0.05
Min	4	1	6.6	9.5	0.5	3.7	0.5
Mean	8	3.5	10.8	31	1.3	5.8	-

663

664

665 **Figure 6**

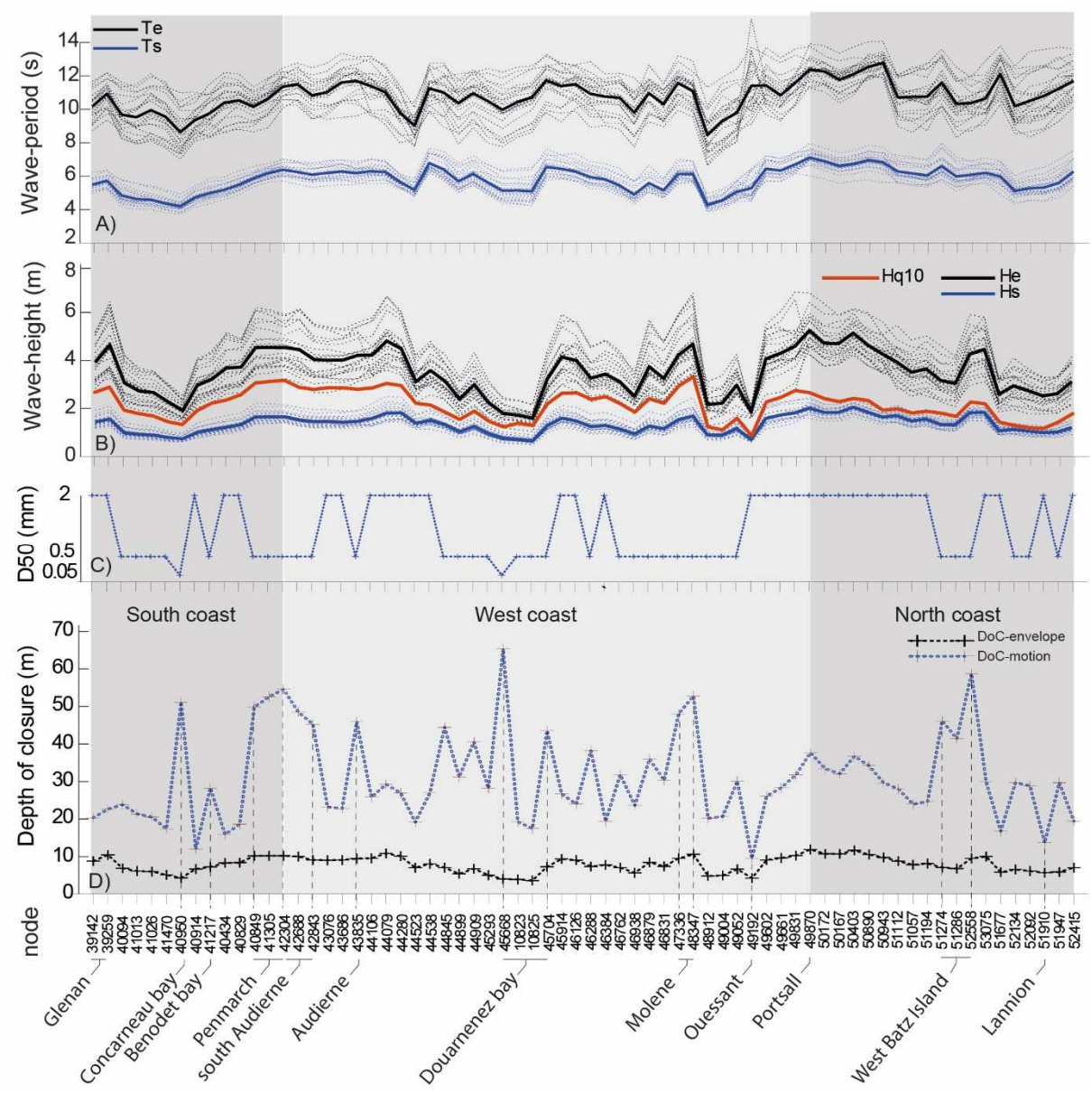

666

667

668 **Figure 7**

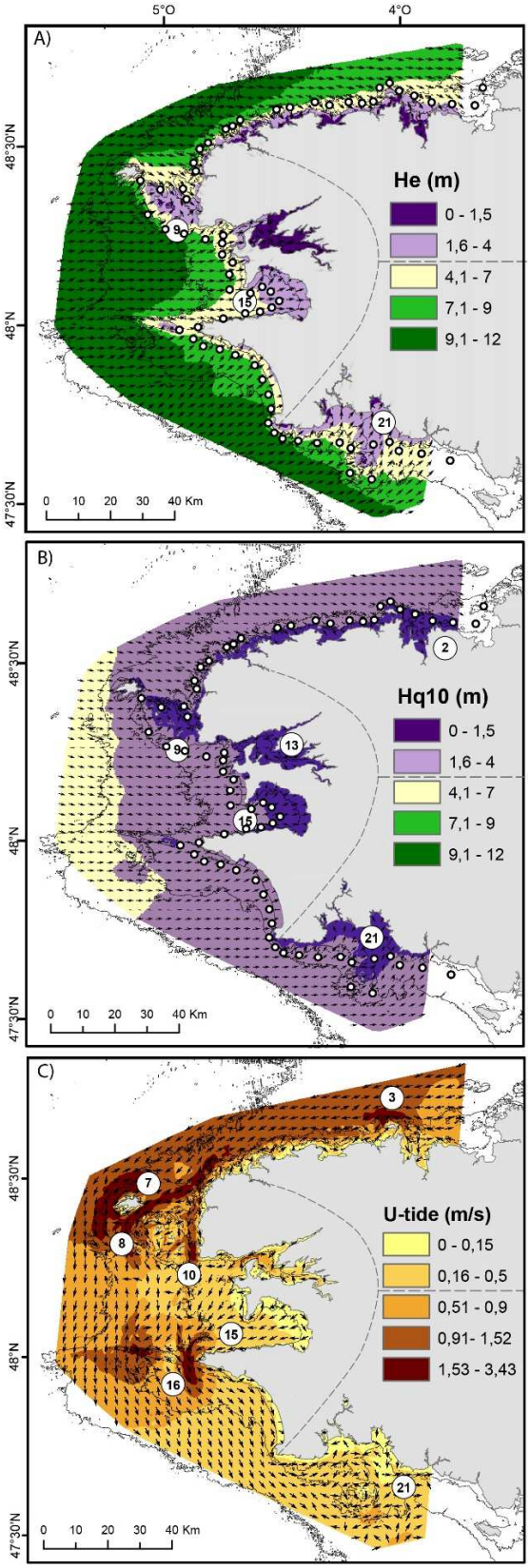

669

670

671 **Figure 8**

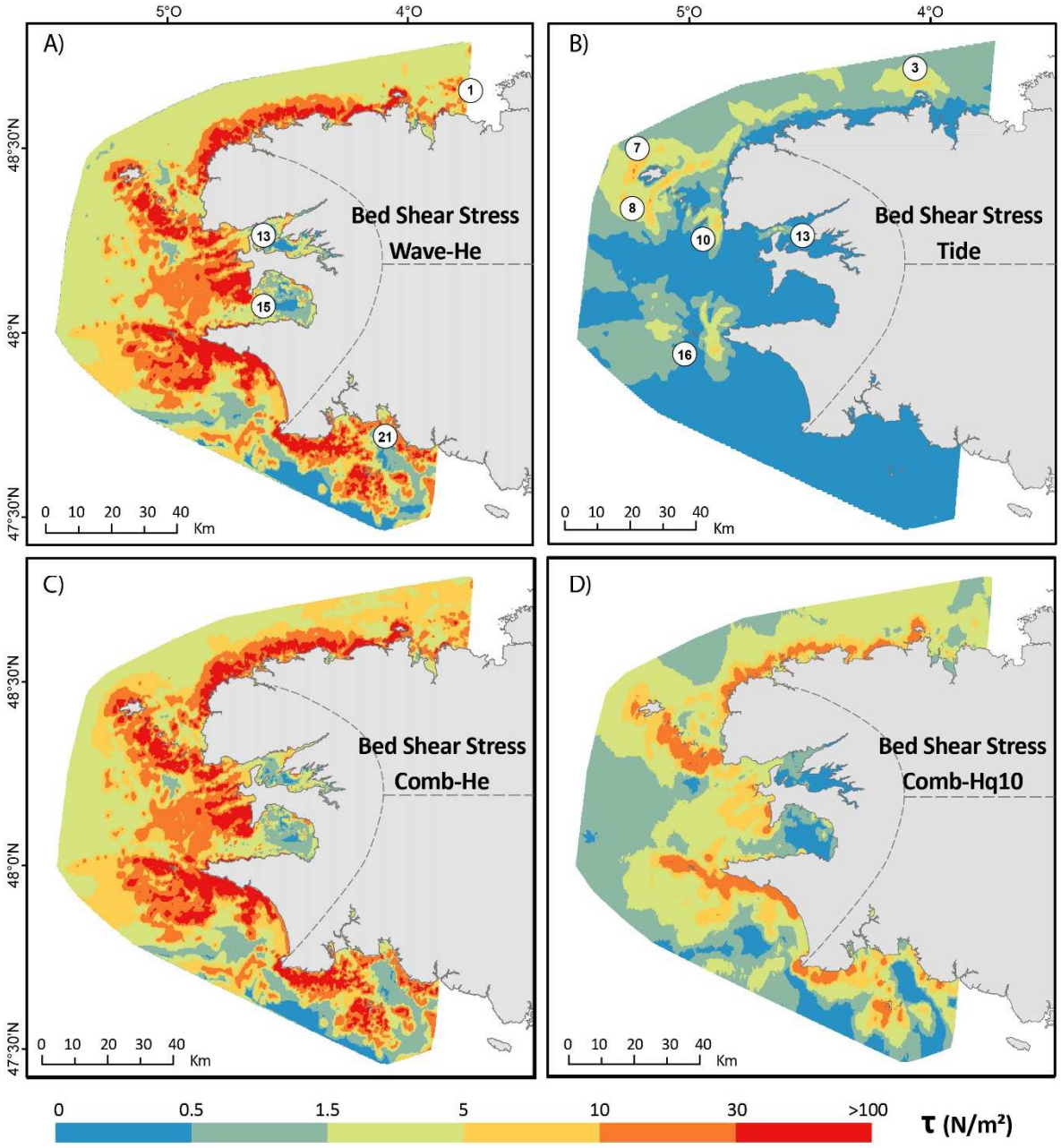

672

673

674

675 **Figure 9**

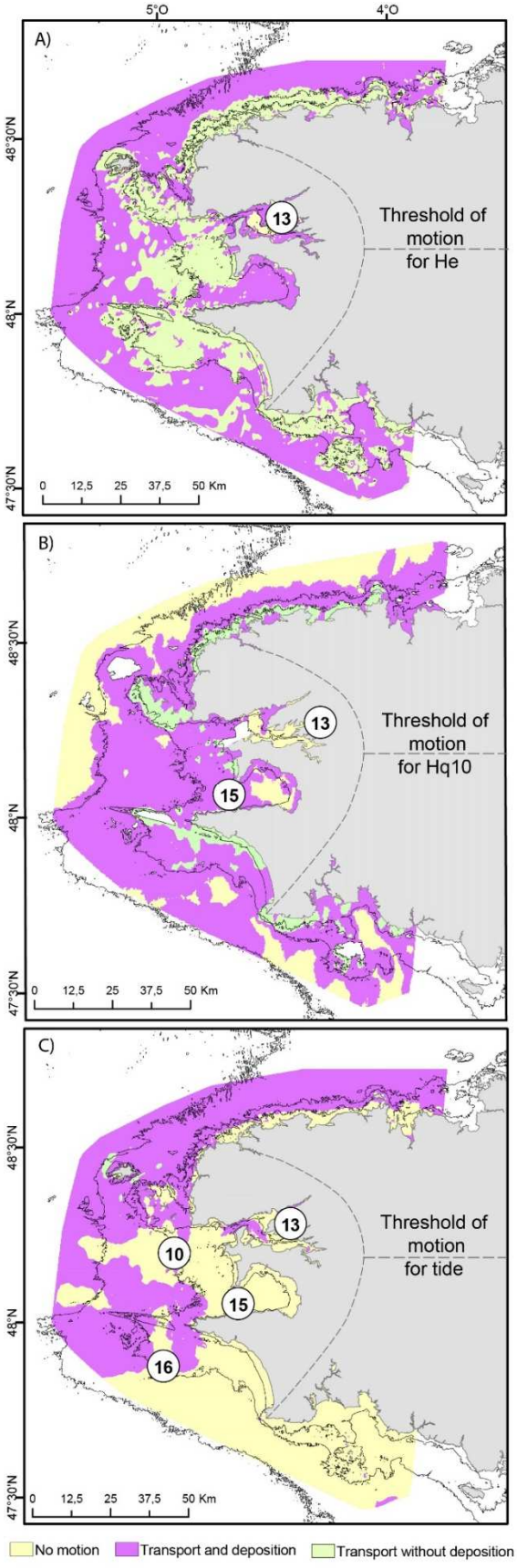

676

677

678 **Figure 10**

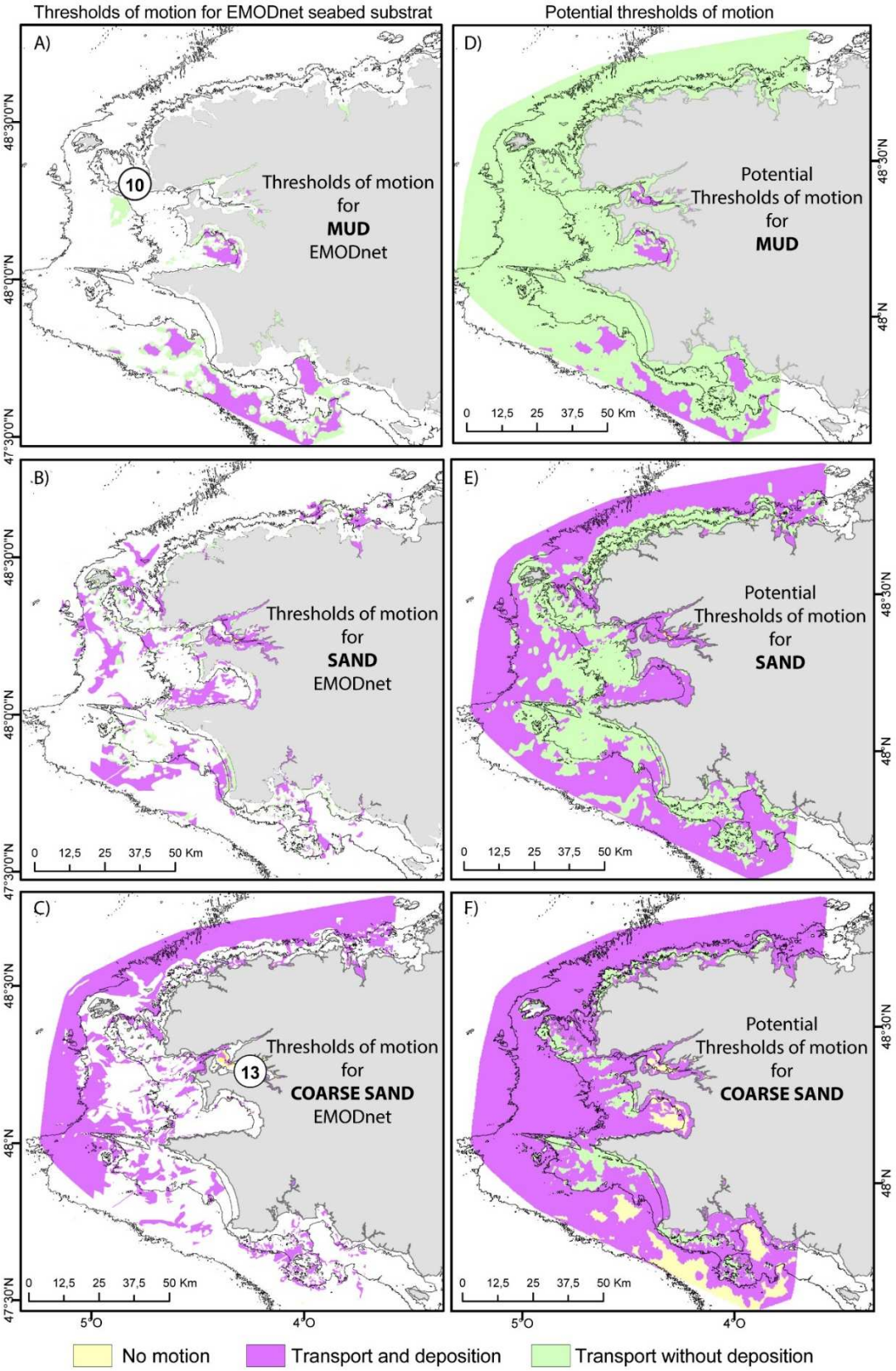

679

680

681 **Figure 11**

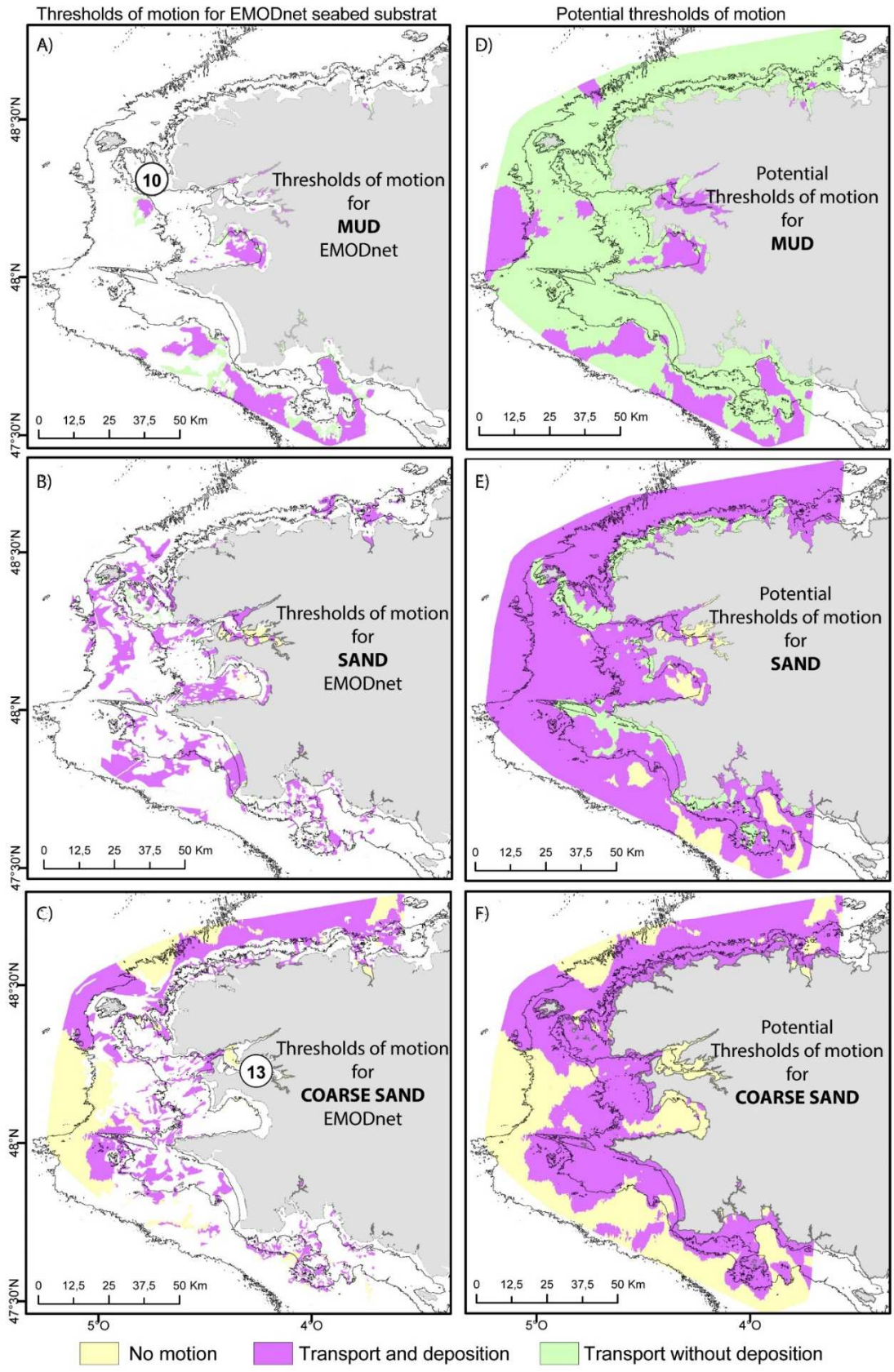

682

683

684 . **Figure 12**

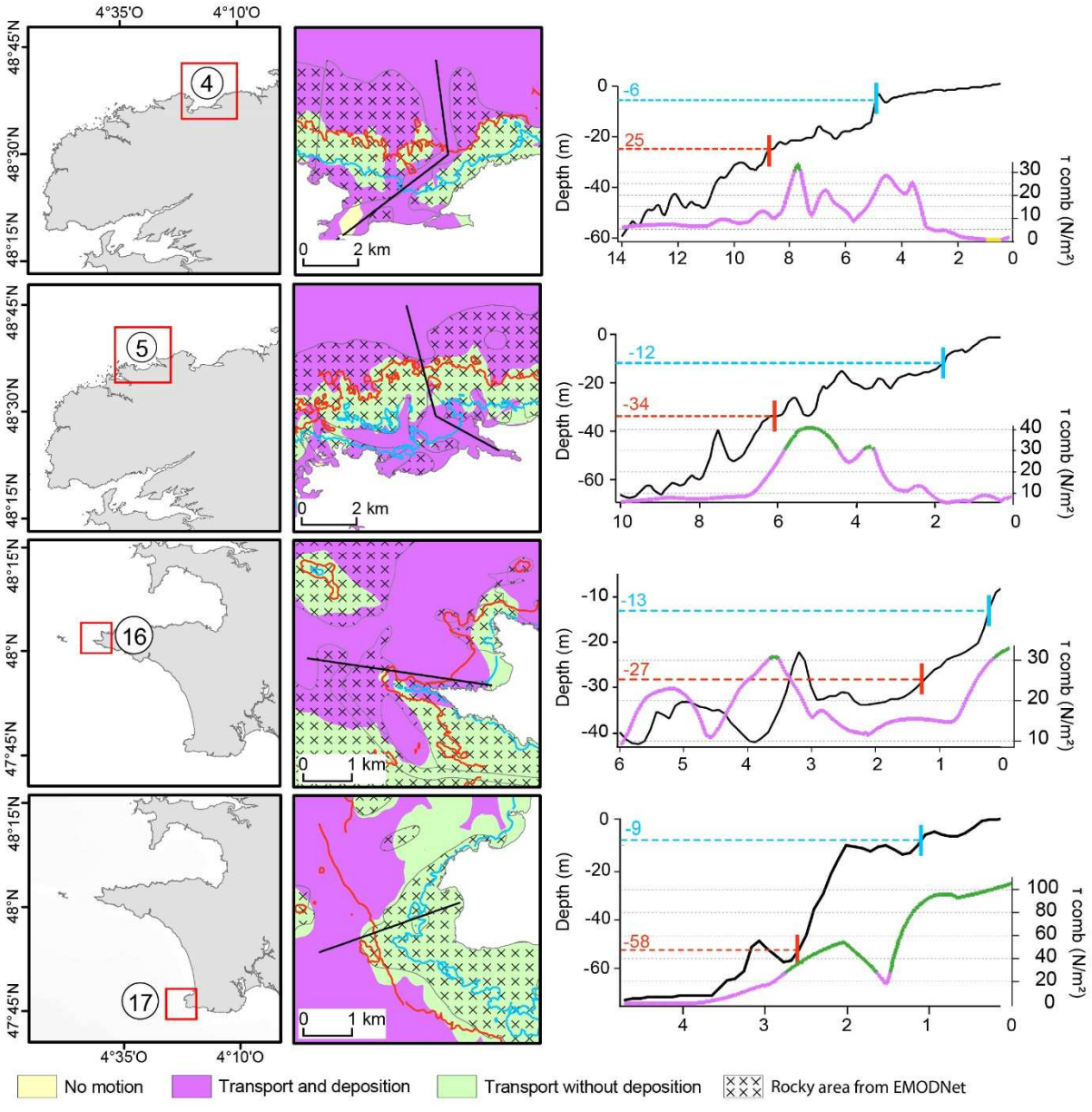

685

686

687 **Table 4**

Autors	Study area	Tide	Mean wave height (m)	Wave period (s)	D50 (mm)	DoC-envelope (m)	DoC-motion (m)
This study	Western Brittany	macro	Hs: 2.1 He: 5.3	Ts: 5 Te: 10	0.5	7.2	35.3
Hamon-Kerivel et al., (2022) Ireland	Bellmullet	macro	He : 5.8	Te: 13.3		15.6	
	Portstewart	macro	He : 2.7	Te: 14.1		7.5	
	Dingle Bay	macro	He : 3.3	Te: 13.4		9.8	
Valiente et al. (2019)	South West England	macro	Hs: 1.6 He: 8.8	Ts: 10 Te: 18.2	0.4	from 18.8 to 23.3	from 33.7 to 50.1
Menier et al. (2019)	South Brittany	meso	Hs < 2.5	Ts < 9	0.5	7	20
De Figueiredo et al. (2019)	Southern Brazil	micro	Hs: 1.07 He: 3.45	Ts: 9.8 Te: 13.8	0.8	from 4.7 to 6.2	from 35.7 to 42.1
Do et al. (2019)	South Korea	micro	He: 3.9	Te: 9.6		7.7	-
Robertson et al. (2008)	South Florida Atlantic Coast	micro	He : from 6 to 9	Te: from 9 to 10		from 12 to 16	-
Nicholls et al. (1998)	North Carolina - USA	micro	He: 1 +/- 0.6	Te: 8.3 +/- 2.6		from 2.7 to 7.8	-

688
689

Figure 13

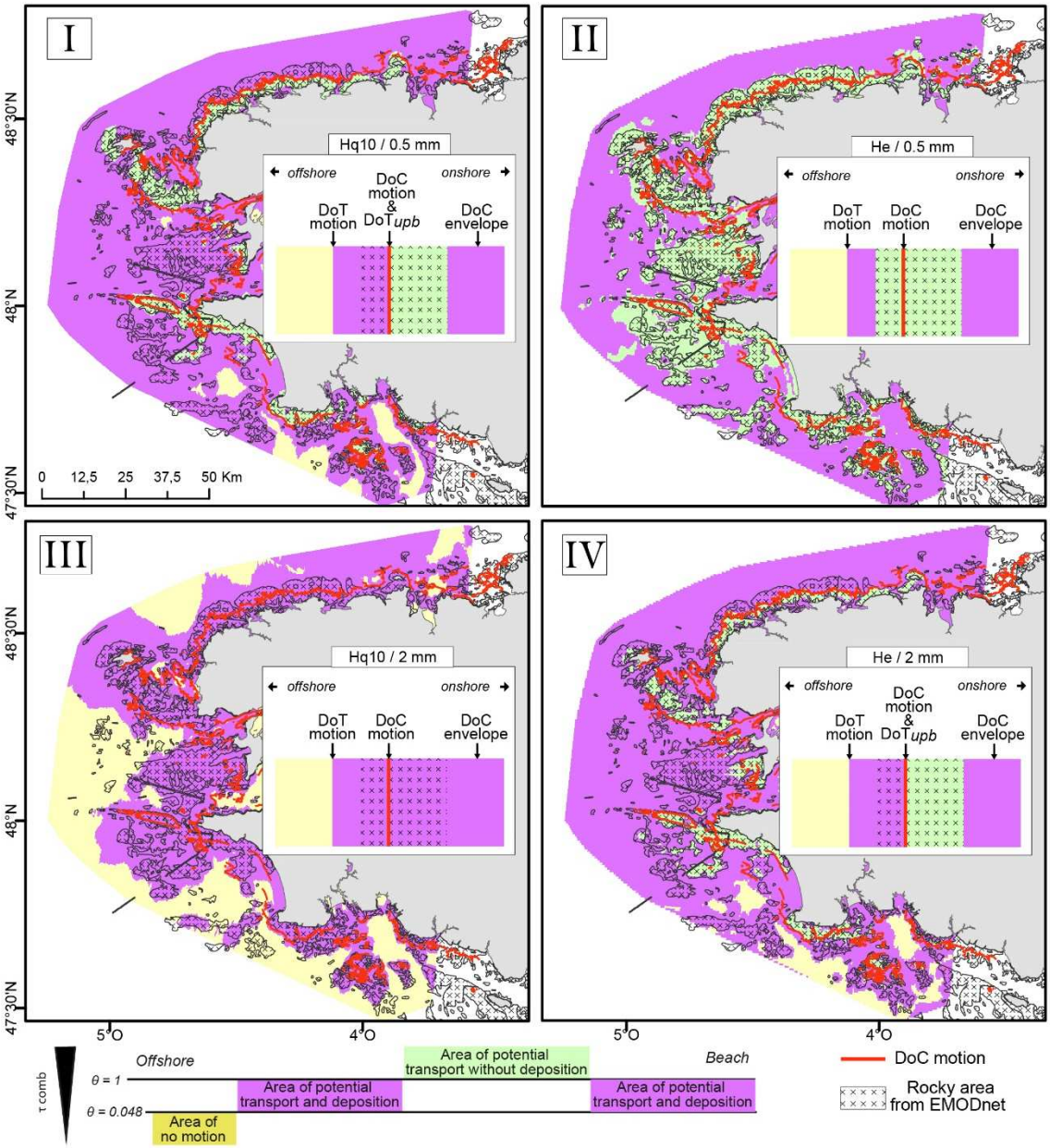
I
II
III
IV
Hq10 / 0.5 mm
He / 0.5 mm
Hq10 / 2 mm
He / 2 mm
offshore
onshore
DoT motion
DoC motion & DoTupb
DoC envelope
48°30'N
48°N
47°30'N
0 12,5 25 37,5 50 Km
5°O
4°O
Offshore
Beach
θ = 1
θ = 0.048
τ comb
Area of potential transport without deposition
Area of potential transport and deposition
Area of potential transport and deposition
Area of no motion
DoC motion
Rocky area from EMODnet

695 **Figure 14**

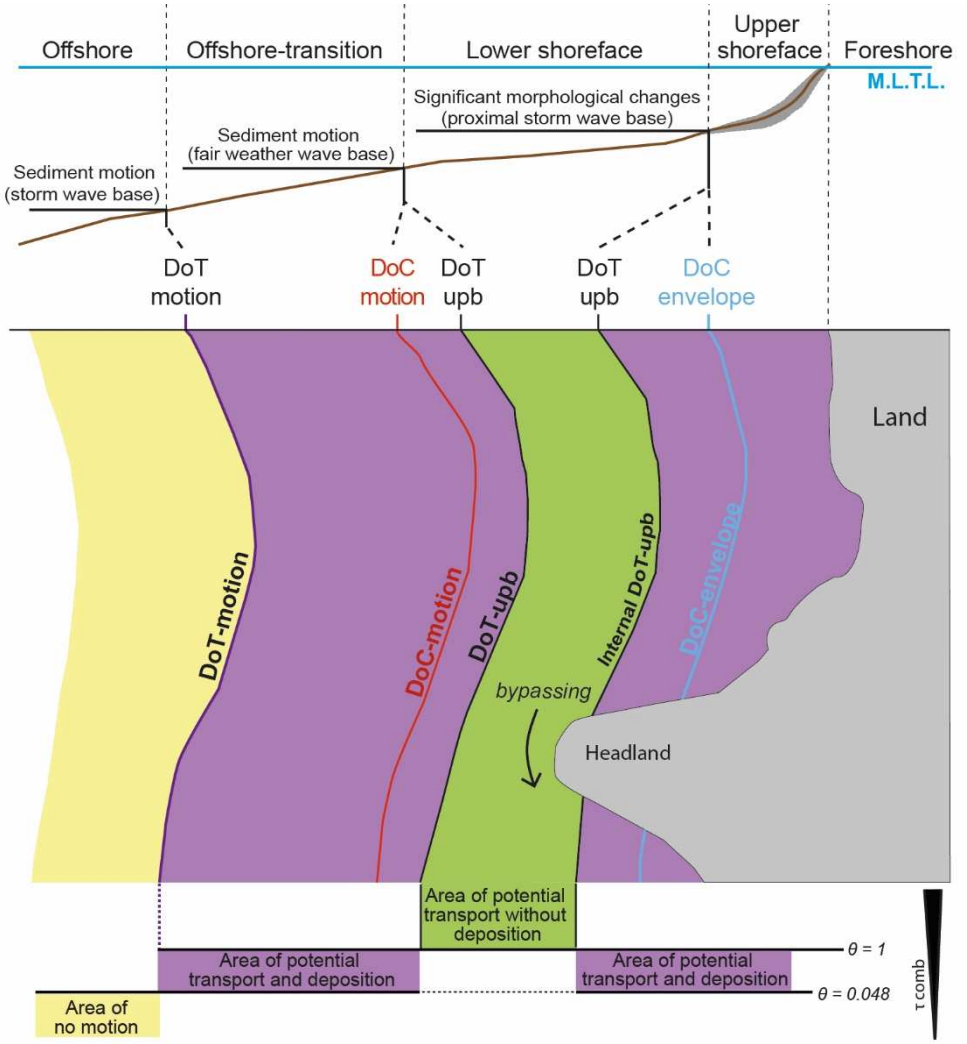

696

697

698

699

700 **Data Availability**

701 Wave data provided by data base HOMERE - IFREMER - Laboratoire Comportement des
702 Structures en Mer and Laboratoire Spatial et Interfaces Air-Mer and can be accessed at
703 https://doi.org/10.12770/cf47e08d-1455-4254-955e-d66225c9dc90 (HOMERE) ; Newly
704 accessible from the Resourcecode marine data toolbox (https://resourcecode.ifremer.fr/). Tide
705 data provided by MARS3D (AGRIF) model simulations, « Modelling and Analysis for
706 Coastal Research » (MARC) project (https://marc.ifremer.fr), Ifremer, University of Brest,
707 CNRS, IRD, Laboratoire d'Océanographie Physique et Spatiale (LOPS), IUEM, Brest,
708 France, and can be accessed at https://doi.org/10.12770/3edee80f-5a3e-42f4-9427-
709 9684073c87f5. The median particle size (D50) data product have been derived from the
710 EMODnet Geology (Seabed Substrates) data portal (www.emodnet-geology.eu/). Bathymetric
711 data for profiles provide by SHOM, 2015 ; MNT Bathymétrique de façade Atlantique (Projet
712 Homonim). http://dx.doi.org/10.17183/MNT_ATL100m_HOMONIM_WGS84".

713

714 **Acknowledgement**

715 This research was supported by the University of Brest- France (University of Bretagne
716 Occidentale - UBO).

717

718 **Figure and table caption**

719 Figure 1: Delineation of the shoreface based on the work of Reading (1996), Cowell et al.
720 (1999) and Nichols (2009), associated with the depth of closure (DoC-motion and envelope)
721 and transport (DoT-upper plan bed: upb) based on the review of Hamon-Kerivel (2020).

722

Figure 2: Western Brittany study area (France). Wave roses (Hs) represent a 23 year (1994-2016) record from WAVEWATCH III® model for the three blue dots. Black solid lines represent mean spring tidal range (cm) from Data Shom (Service Hydrographique et Océanographique de la Marine). Numbers (1) to (22) correspond to the location of the specific areas studied.

Figure 3: Seabed substrate and sediment data from The European Marine Observation and Data Network (EMODnet, Geology, 2016); 1/ 250 000 scale, using Folk 5 class classification. Isobaths -30 m, -50 m and -100 m are indicated with black lines. The numbers correspond to the name of the areas detailed in the text; see Figure 2 for location.

Table 1: Threshold bed shear stress for different grain sizes and for the two values of Shields mobility numbers indicating transport initiation and transition to the upper plane bed.

Figure 4: Flow diagram of the methodology for the calculation of the Depths of Closure (DoC_{env} and DoC_{motion}) and Depth of Transport (DoT_{motion} and DoT_{upb} - upper plane bed) from hydrodynamic and sedimentary databases. LST (Large Spring Tide) and LWS (Low water spring). τwave (τw) and τtide(τt) correspond respectively to wave and tide bed shear shear. τmean (τm) and τcomb correspond respectively to mean and combined bed shear.

Figure 5: Left panel: map of the HOMERE nodes extent for wave parameters (black and grey dots) and MARS3D grid extent for tide parameters. White dots indicate nodes selected for DoCs (DoC_{env} and DoC_{motion}) formulations and grey dots indicate the selected nodes for DoT formulation. Right panel: Identification numbers of the HOMERE nodes (WAVEWATCH III® model) for DoCs (DoC_{env} and DoC_{motion}) calculations.

748

749 Table 2: EMODnet Seabed substrate and associated grain size (D50) used in this study.

750

751 Table 3: Maximum, minimum, and mean values of DoC_{env} and DoC_{motion} with associated
752 wave parameters and grain sizes.

753

754 Figure 6: Depth of closure envelope and motion for 68 nodes along the western Brittany coast
755 (D) with associated wave heights and periods, and grain sizes (D50) (A, B, C). Blues lines
756 indicate the DoC_{motion} results and associated parameters Hs, Ts, and D50. Black lines indicate
757 the DoC_{env} results and associated parameters He and Te. Dotted black and blue lines represent
758 wave heights and periods year by year from 1994 to 2016 (graphs A and B). Bold black and
759 blue lines represent mean of wave heights and periods from 1994 to 2016 (graphs A and B).
760 The red line represents Hq10. See Figure 5 for location of nodes.

761

762 Figure 7: Wave heights and directions (arrows) during: A) extreme conditions He (wave
763 heights exceeded for 12 hours for February 2014); B) moderate conditions Hq10 (10^{th}
764 percentile of He). Friction velocity (m/s) and direction of maximum tidal currents near the
765 bottom (C). Data from WAVEWATCH III® model (HOMERE dabatase) and MARS3D
766 models, respectively. White dots indicate nodes for wave parameter taken into account for the
767 DoCs calculations, see Figure 6. The numbers correspond to the name of the specific area
768 studied; see Figure 2 for location. Thin black lines are isobaths -20 m, -50 m, -100 m. Grey
769 dotted lines represent the north/west/south limits.

770

771 Figure 8: Western Brittany bed shear stress due to extreme waves (A), tide (B), combined bed
772 shear stress during extreme wave conditions He (C), and combined bed shear stress during

773 moderated wave conditions Hq10 (D). Grey dotted lines represent the north/west/south limits.
774 The numbers correspond to the name of the specific area studied; see Figure 2 for location.
775
776 Figure 9: Threshold of motion (from DoT formulation) for: A) extreme wave alone (He); B)
777 moderated wave alone (Hq10) and C) tide alone, for a grain size of 0.5 mm. Thin black lines
778 are isobaths -20 m, - 50 m, -100 m. The numbers correspond to the name of the specific area
779 studied; see Figure 2 for location. Grey dotted lines represent the north/west/south limits.
780
781 Figure 10: Threshold of motion in the case of extreme waves conditions (He) constrained by
782 EMODnet particle size class (Left panels, A-mud ; B-sand ; C-coarse sand) and threshold of
783 motion for potential sediment transport of a single size class over the entire area (Right
784 panels, D-mud ; E-sand ; F-coarse sand). Thin black lines are isobaths -20 m, - 50 m, -100 m.
785 The numbers correspond to the name of the specific area studied; see Figure 2 for location.
786
787 Figure 11: Threshold of motion in the case of moderate wave conditions (Hq10) constrained
788 by EMODnet particle size class (Left panels, A-mud ; B-sand ; C-coarse sand) and threshold
789 of motion for potential sediment transport of a single size class over the entire area (Right
790 panels, D-mud ; E-sand ; F-coarse sand). Thin black lines are isobaths -20 m, - 50 m, -100 m.
791 The numbers correspond to the name of the specific area studied; see Figure 2 for location.
792
793 Figure 12: Zooms on potential ATD obtained following the DoT approach during extreme
794 conditions (He) (D50 = 2mm) for Goulven (4), Guisseny (5), Sein (16), and Penmarc'h (18)
795 areas (localisation in left panels). Profiles represent the morphology (left axis, black lines) of
796 the seabed (SHOM, 2015, 100m) with DoC limits (red and blue lines represent the DoC_{motion}

797 and the DoC_{env} respectively) and ATDc (purple line) as well as the combined bed shear stress
798 (Right axis). Black cross symbols represent the rocky areas from EMODnet data.
799
800 Table 4: DoC_{env} and DoC_{motion} (Hallermeier 1978 and 1981) and input parameters (height and
801 period of wave and grain size) for several studies of the macro to micro tidal environment.
802
803 Figure 13: Scenario from I to IV of the sediment mobility sequence in accordance with grain
804 sizes (0.5 mm and 2 mm), depth of closure motion (DoC_{motion}) and rocky area from
805 EMODnet, during the moderated period (I and III) and the extreme period (II and IV).
806
807 Figure 14: Definition of the shoreface (modified after Reading, 1996 and Cowell et al., 1999)
808 associated with the depths of closure DoC (Hallermeier, 1978 and 1981) and DoT_{upb} (Valiente
809 et al., 2019). Dashed black lines represent the spatial variability of DoC_{motion} and transport
810 without deposit area. The brown line represents the seabed and the grey envelope represents
811 the significant changes in beach profile. MLTL (Mean Low Tide Level) and upb (upper plan
812 bed).
813
814
815 **References**
816 Aagaard, T., 2011. Sediment transfer from beach to shoreface: The sediment budget of an
817 accreting beach on the Danish North Sea Coast. Geomorphology 135, 143–157.
818 https://doi.org/10.1016/j.geomorph.2011.08.012
819 Allen, J.R.L., 1968. The Nature and Origin of Bed-Form Hierarchies. Sedimentology 10, 161–
820 182. https://doi.org/10.1111/j.1365-3091.1968.tb01110.x

821 Anthony, E.J., Aagaard, T., 2020. The lower shoreface: Morphodynamics and sediment
822 connectivity with the upper shoreface and beach. Earth-Science Reviews 210, 103334.
823 https://doi.org/10.1016/j.earscirev.2020.103334
824 Aragonés, L., Pagán, J.I., López, I., Serra, J.C., 2018. Depth of closure: New calculation
825 method based on sediment data. International Journal of Sediment Research 33, 198–207.
826 https://doi.org/10.1016/j.ijsrc.2017.12.001
827 Aragonés, L., Pagán, J.I., López, M.P., Serra, J.C., 2019. Cross-shore sediment transport
828 quantification on depth of closure calculation from profile surveys. Coastal Engineering
829 151, 64–77. https://doi.org/10.1016/j.coastaleng.2019.04.002
830 Barnard, P.L., Schoellhamer, D.H., Jaffe, B.E., McKee, L.J., 2013. Sediment transport in the
831 San Francisco Bay Coastal System: An overview. Marine Geology 345, 3–17.
832 https://doi.org/10.1016/j.margeo.2013.04.005
833 Birkemeier, W.A., Asce, A.M., 1985. Field Data on Seaward Limit of Profile Change. Journal
834 of Waterway, Port, Coastal, and Ocean Engineering 3, 598–602.
835 Blaise, E., Suanez, S., Stéphan, P., Fichaut, B., David, L., Cuq, V., Autret, R., Houron, J.,
836 Rouan, M., Floc'h, F., Ardhuin, F., Cancouët, R., Davidson, R., Costa, S., Delacourt, C.,
837 2015. Bilan des tempêtes de l'hiver 2013-2014 sur la dynamique de recul du trait de côte
838 en Bretagne. Géomorphologie : relief, processus, environnement 21, 267–292.
839 https://doi.org/10.4000/geomorphologie.11104
840 Bonnefille, R., 1994. Mouvements de la mer, 3rd ed. Ed. Techniques Ingénieur.
841 Boudière, E., Maisondieu, C., Ardhuin, F., Accensi, M., Pineau-Guillou, L., Lepesqueur, J.,
842 2013. A suitable metocean hindcast database for the design of Marine energy converters.
843 International Journal of Marine Energy, Special Issue – Selected Papers - EWTEC2013 3–
844 4, e40–e52. https://doi.org/10.1016/j.ijome.2013.11.010

Cagnard, F., 2008. Carte géologiques harmonisée du département du Finistère BRGM : RP-56273 - FR.

Capobianco, M., Hanson, H., Larson, M., Steetzel, H., Stive, M.J.F., Chatelus, Y., Aarninkhof, S., Karambas, T., 2002. Nourishment design and evaluation: applicability of model concepts. Coastal Engineering 47, 113–135.

Cerkowniak, G., Ostrowski, R., Stella-Bogusz, M., 2015. Depth of closure in the multi-bar non-tidal nearshore zone of the Baltic Sea: Lubiatowo (Poland) case study. Bulletin of the Maritime Institute in Gdańsk 30, 180–188. https://doi.org/10.5604/12307424.1185577

Chauris, L., 1987. Le sphène : Un minéral-traceur. L'exemple des sables lourds des plages du Nord-Finistère (France). Comptes Rendus de l'Académie des Sciences, Paris 305, 27–30.

Coughlan, M., Guerrini, M., Creane, S., O'Shea, M., Ward, S.L., Van Landeghem, K.J.J., Murphy, J., Doherty, P., 2021. A new seabed mobility index for the Irish Sea: Modelling seabed shear stress and classifying sediment mobilisation to help predict erosion, deposition, and sediment distribution. Continental Shelf Research 229, 104574. https://doi.org/10.1016/j.csr.2021.104574

Cowell, P.J., Hanslow, D.J., Meleo, J.F., 1999. The Shoreface. In : Short,A.D.,(ed.), in: Handbook of Beach and Shoreface Morphodynamics. Chichester, pp. 39–71.

Cowell, P.J., Stive, M.J.F., Niedoroda, A.W., Swift, D.J.P., de Vriend, H.J., Buijsman, M.C., Nicholls, R.J., Roy, P.S., Kaminsky, G.M., Cleveringa, J., Reed, C.W., de Boer, P.L., 2003. The Coastal-Tract (Part 2): Applications of Aggregated Modeling of Lower-order Coastal Change. Journal of Coastal Research 19, 21.

De Figueiredo, S.A., Goulart, E.S., Calliari, L.J., 2020. Effects of closure depth changes on coastal response to sea level rise: Insights from model experiments in southern Brazil. Geomorphology 351, 106935. https://doi.org/10.1016/j.geomorph.2019.106935

869 Do, J.D., Jin, J.-Y., Jeong, W.M., Chang, Y.S., 2019. Observation of Rapid Seabed Erosion
870 Near Closure Depth During a Storm Period at Hujeong Beach, South Korea. Geophysical
871 Research Letters 46, 9804–9812. https://doi.org/10.1029/2019GL083910
872 Grant, W.D., Madsen, O.S., 1982. Movable bed roughness in unsteady oscillatory flow. Journal
873 of Geophysical Research: Oceans 87, 469–481. https://doi.org/10.1029/JC087iC01p00469
874 Gregoire, G., 2016. Dynamique sédimentaire et évolution holocène d'un système macrotidal
875 semi-fermé : l'exemple de la rade de Brest (phdthesis). Université de Bretagne occidentale
876 - Brest.
877 Hallermeier, R.J., 1981. A profile zonation for seasonal sand beaches from wave climate.
878 Coastal Engineering 4, 253–277. https://doi.org/10.1016/0378-3839(80)90022-8
879 Hallermeier, R.J., 1978. Uses for a Calculated Limit Depth to Beach Erosion. Coastal
880 Engineering 1493–1512. https://doi.org/10.1061/9780872621909.090
881 Hamon-Kerivel, K., Cooper, A., Jackson, D., Sedrati, M., Guisado Pintado, E., 2020. Shoreface
882 mesoscale morphodynamics: A review. Earth-Science Reviews 209, 103330.
883 https://doi.org/10.1016/j.earscirev.2020.103330
884 Hamon-Kerivel, K., Jackson, D., Pintado, E.G., Cooper, A., Sedrati, M., 2022. Spatial and
885 temporal variability of shorefaces: A morpho-hydrodynamic controlled system. Estuarine,
886 Coastal and Shelf Science 108162. https://doi.org/10.1016/j.ecss.2022.108162
887 Helland-Hansen, W., Steel, R.J., Sømme, T.O., 2012. Shelf genesis revisited. Journal of
888 Sedimentary Research 82, 133–148. https://doi.org/10.2110/jsr.2012.15
889 Hénaff, A., Lageat, Y., Hallégouët, B., Jabbar, M., Delliou, N., Diard, M., 2015. Évolutions des
890 accumulations littorales et relations avec les dynamiques d'avant-plage dans l'archipel des
891 Glénan (Sud-Finistère, France). Géomorphologie : relief, processus, environnement 21,
892 359–384. https://doi.org/10.4000/geomorphologie.11195

Héquette, A., Aernouts, D., 2010. The influence of nearshore sand bank dynamics on shoreline evolution in a macrotidal coastal environment, Calais, northern France. Continental Shelf Research 30, 1349–1361. https://doi.org/10.1016/j.csr.2010.04.017

Hinschberger, F., Saint-Réquier, A., 1970. Les sédiments vaseux au large du Finistère. Norois 67, 401–403. https://doi.org/10.3406/noroi.1970.7345

Jabbar, M., 2016. Dynamiques morpho-sédimentaires des avant-plages et impact sur les stocks sableux : vers une meilleure stratégie de gestion des risques côtiers.

Jabbar, M., Hénaff, A., Deschamps, A., 2015. Dynamiques et évolutions morpho-sédimentaires de l'avant-plage du secteur littoral de Combrit – Île-Tudy entre le XIXe et le XXIe siècle. Géomorphologie : relief, processus, environnement 21, 45–56. https://doi.org/10.4000/geomorphologie.10849

King, E.V., Conley, D.C., Masselink, G., Leonardi, N., McCarroll, R.J., Scott, T., Valiente, N.G., 2021. Wave, Tide and Topographical Controls on Headland Sand Bypassing. J. Geophys. Res. Oceans 126. https://doi.org/10.1029/2020JC017053

Klein, A.H.F., Vieira da Silva, G., Taborda, R., da Silva, A.P., Short, A.D., 2020. 23 - Headland bypassing and overpassing: form, processes and applications, in: Jackson, D.W.T., Short, A.D. (Eds.), Sandy Beach Morphodynamics. Elsevier, pp. 557–591. https://doi.org/10.1016/B978-0-08-102927-5.00023-0

Komar, P.D., 1996. Tidal-Inlet Processes and Morphology Related to the Transport of Sediments. Journal of Coastal Research, 23–45.

Latteux, B., 2008. Exploitation de matériaux marins et stabilité du littoral, Quae. ed, Savoir faire. Versailles.

Lazure, P., Dumas, F., 2008. An external–internal mode coupling for a 3D hydrodynamical model for applications at regional scale (MARS). Advances in Water Resources 31, 233–250. https://doi.org/10.1016/j.advwatres.2007.06.010

Luijendijk, A., Hagenaars, G., Ranasinghe, R., Baart, F., Donchyts, G., Aarninkhof, S., 2018. The State of the World's Beaches. Sci Rep 8, 1–11. https://doi.org/10.1038/s41598-018-24630-6

Marsh, S.W., Nicholls, R.J., Kroon, A., Hoekstra, P., 1998. Assessment of Depth of Closure on a Nourished Beach: Terschelling, The Netherlands, in: Coastal Engineering 1998. Presented at the 26th International Conference on Coastal Engineering, American Society of Civil Engineers, Copenhagen, Denmark, pp. 3110–3123. https://doi.org/10.1061/9780784404119.236

McCarroll, R.J., Masselink, G., Valiente, N.G., King, E.V., Scott, T., Stokes, C., Wiggins, M., 2021. An XBeach derived parametric expression for headland bypassing. Coastal Engineering 165, 103860. https://doi.org/10.1016/j.coastaleng.2021.103860

McCarroll, R.J., Masselink, G., Valiente, N.G., Scott, T., King, E.V., Conley, D., 2018. Wave and Tidal Controls on Embayment Circulation and Headland Bypassing for an Exposed, Macrotidal Site. Journal of Marine Science and Engineering 6, 94. https://doi.org/10.3390/jmse6030094

Mengual, B., Le Hir, P., Cayocca, F., Garlan, T., 2019. Bottom trawling contribution to the spatio-temporal variability of sediment fluxes on the continental shelf of the Bay of Biscay (France). Marine Geology 414, 77–91. https://doi.org/10.1016/j.margeo.2019.05.009

Menier, D., Mathew, M., Cherfils, J.-B., Ramkumar, M., Estournès, G., Koch, M., Guillocheau, F., Sedrati, M., Goubert, E., Gensac, E., Le Gall†, R., Novico, F., 2019. Holocene Sediment Mobilization in the Inner Continental Shelf of the Bay of Biscay: Implications for Regional Sediment Budget Offshore to Onshore. Journal of Coastal Research 88, 110. https://doi.org/10.2112/SI88-009.1

Meyer-Peter, E., Müller, R., 1948. Formulas for Bed-Load transport. IAHSR 2nd meeting, Stockholm, appendix 2.

943 Maisondieu, C., Accensi, M., Le Roux, J.-F., Boudière, E., 2017. Manuel de l'utilisateur de la
944 base de données HOMERE, Mise à jour 2017 du jeu de données de hindcast. Ifremer.
945 Moss, A.J., 1972. Bed-Load Sediments. Sedimentology 18, 159–219.
946 https://doi.org/10.1111/j.1365-3091.1972.tb00012.x
947 Musset, R., 1934. La formation du réseau hydrographique de la Bretagne occidentale. Annales
948 de géographie 43, 561–578. https://doi.org/10.3406/geo.1934.10729
949 Nicholls, R.J., Birkemeier, W.A., Hallermeier, R.J., 1997. Application of the Depth of Closure
950 Concept, in: Coastal Engineering 1996. Presented at the 25th International Conference on
951 Coastal Engineering, American Society of Civil Engineers, Orlando, Florida, United
952 States, pp. 3874–3887. https://doi.org/10.1061/9780784402429.299
953 Nicholls, R.J., Birkemeier, W.A., Lee, G., 1998. Evaluation of depth of closure using data from
954 Duck, NC, USA. Marine Geology 148, 179–201. https://doi.org/10.1016/S0025-
955 3227(98)00011-5
956 Nichols, G., 2009. Sedimentology and Stratigraphy. John Wiley & Sons.
957 Ortiz, A.C., Ashton, A.D., 2016. Exploring shoreface dynamics and a mechanistic explanation
958 for a morphodynamic depth of closure. Journal of Geophysical Research: Earth Surface
959 121, 442–464. https://doi.org/10.1002/2015JF003699
960 Parker, G., Seminara, G., Solari, L., 2003. Bed load at low Shields stress on arbitrarily sloping
961 beds: Alternative entrainment formulation. Water Resources Research 39.
962 https://doi.org/10.1029/2001WR001253
963 Pinot, J.P., 1998. La gestion du littoral. Tome 1 : Littoraux tempérés : côtes rocheuses et
964 sableuses. Institut Océanographique, Paris.
965 Preston, J., Hurst, M.D., Mudd, S.M., Goodwin, G.C.H., Newton, A.J., Dugmore, A.J., 2018.
966 Sediment accumulation in embayments controlled by bathymetric slope and wave energy:

967 Implications for beach formation and persistence. Earth Surface Processes and Landforms
968 43, 2421–2434. https://doi.org/10.1002/esp.4405
969 Reading, H.G., 1996. Sedimentary environments: processes, facies, and stratigraphy, 3rd ed.
970 Wiley -Blackwell, Cambridge, Mass.
971 Robertson, W., Zhang, K., Finkl, C.W., Whitman, D., 2008. Hydrodynamic and geologic
972 influence of event-dependent depth of closure along the South Florida Atlantic Coast.
973 Marine Geology 252, 156–165. https://doi.org/10.1016/j.margeo.2008.03.018
974 Rozynski, G., Pruszak, Z., Okroj, T., Zeidler, R., 1998. Depth of closure and seabed variability
975 patterns. Coastal Engineering Proceedings 1.
976 Shields, A., 1936. Application of similarity principles and turbulence research to bed-load
977 movement.
978 Silva, A.P. da, Vieira da Silva, G., Strauss, D., Murray, T., Woortmann, L.G., Taber, J.,
979 Cartwright, N., Tomlinson, R., 2021. Headland bypassing timescales: Processes and
980 driving forces. Science of The Total Environment 793, 148591.
981 https://doi.org/10.1016/j.scitotenv.2021.148591
982 Soulsby, R.L., 1997. Dynamics of marine sands: a manual for practical applications.
983 Oceanographic Literature Review 9, 947.
984 Southard, J.B., Boguchwal, L.A., 1990. Bed configuration in steady unidirectional water flows;
985 Part 2, Synthesis of flume data. Journal of Sedimentary Research 60, 658–679.
986 https://doi.org/10.1306/212F9241-2B24-11D7-8648000102C1865D
987 Stéphan, P., Blaise, E., Suanez, S.S., Fichaut, B., Autret, R., Floc'H, F., Madec Cuq, V., Le
988 Dantec, N., Ammann, J., David, L., Jaud, M., Delacourt, C., 2019. Long, medium, and
989 short-term shoreline dynamics of the Brittany coast (Western France). Journal of Coastal
990 Research Special Issue No. 88, 89–109. https://doi.org/10.2112/SI88-008.1

991 Stive, M.J.F., de Vriend, H.J., 1995. Modelling shoreface profile evolution. Marine Geology
992 126, 235–248. https://doi.org/10.1016/0025-3227(95)00080-I
993 Udo, K., Ranasinghe, R., Takeda, Y., 2020. An assessment of measured and computed depth of
994 closure around Japan. Sci Rep 10, 2987. https://doi.org/10.1038/s41598-020-59718-5
995 Valiente, N.G., Masselink, G., Scott, T., Conley, D., McCarroll, R.J., 2019. Role of waves and
996 tides on depth of closure and potential for headland bypassing. Marine Geology 407, 60–
997 75. https://doi.org/10.1016/j.margeo.2018.10.009
998 Wright, L.D., 1995. Morphodynamics of Inner Continental Shelves, CRC Press, Inc. ed. Boca
999 Rato, Florida.
1000 Yoni, C., Hallégouët, B., 1998. Extractions d'amendements marins et recul de la ligne de
1001 rivage en baie de Goulven (Finistère). Les paradoxes de la gestion d'un site. Norois 177,
1002 63–73. https://doi.org/10.3406/noroi.1998.6850
1003